

1

Supplementary Information

2 Performance Optimization of Solution-processed TADF-OLEDs Using Core- 3 Identical Small, Medium, and High Molecular Weight Hosts

4

5 Shinyoung Kim[¶], Chae Yeong Park[¶], Nagaraju Peethani[¶], Ha Yeon Kim, Haeun Kwak, Subin
6 Kwon, Yesoo Lee, Chang Seop Hong, Sungnam Park, Min Ju Cho*, Dong Hoon Choi*

7

8 Department of Chemistry, Research Institute for Natural Sciences, Korea University,
9 145 Anam-ro, Seongbuk-gu, Seoul 02841, Korea

10

11 *Corresponding authors: M. J. Cho (E-mail: chominju@korea.ac.kr); D. H. Choi (E-mail:
12 dhchoi8803@korea.ac.kr)

13 [¶]S. Kim, C. Y. Park, and P. Nagaraju equally contributed to this work.

14

15 General Information

16 Characterization and measurements

17 All UV-visible absorption spectra of the polymers in toluene solutions and thin films were
18 recorded using a UV-visible absorption spectrometer (Agilent 8453, photodiode array, $\lambda = 190\text{--}1100\text{ nm}$). The fluorescence (77 and 298 K) and phosphorescence (77 K, delay time = 1.0 ms)
19 spectra were recorded using an F-7100 fluorescence spectrophotometer (HITACHI). Proton
20 nuclear magnetic resonance ($^1\text{H NMR}$, 500 MHz) and carbon nuclear magnetic resonance (^{13}C
21 NMR, 125 MHz) spectra were recorded in CDCl_3 using Varian Mercury spectrometers
22 (Cambridge Isotope Laboratories, Inc.). The masses of the synthesized compounds were
23 determined by matrix-assisted laser desorption ionization time-of-flight (MALDI-TOF) mass
24 spectrometry (MALDI-TOF/TOF™ 5800 system, AB SCIEX) at the Korea Basic Science Institute
25

1 (Seoul). Elemental analysis was performed using a FlashSmartTM elemental analyzer (Thermo
2 Fisher Scientific). All electrochemical experiments were conducted using a Biologic VSP3e
3 potentiostat controlled by EC-Lab v11.43 software. The electrochemical properties were
4 characterized through cyclic voltammetry using an electrolyte solution prepared by dissolving
5 tetrabutylammonium hexafluorophosphate (Bu_4NPF_6) in acetonitrile. A Pt wire and Ag/AgCl
6 electrode (3.4 M KCl leak-free 2.0 mm diameter, Innovative Instruments) were used as the counter
7 and reference electrodes, respectively.

8 Time-resolved photoluminescence (TRPL) experiments were carried out by exciting the
9 doped films with a 355-nm pulse at 10 Hz using an Nd:YAG laser (Q-smart 850, Lumibird FR).
10 The TRPL signals were collected using a lens (focal length = 10 cm), passed through a
11 monochromator, and detected using a photomultiplier tube (PMT) connected to a 100-MHz digital
12 oscilloscope (DSO-X 3014A, Keysight).

13 The absolute photoluminescence quantum yields (PLQYs) of the films were determined using
14 an integrating sphere (ILF-835) equipped with an FP-8500 spectrofluorometer (JASCO).

15

16 Theoretical calculations

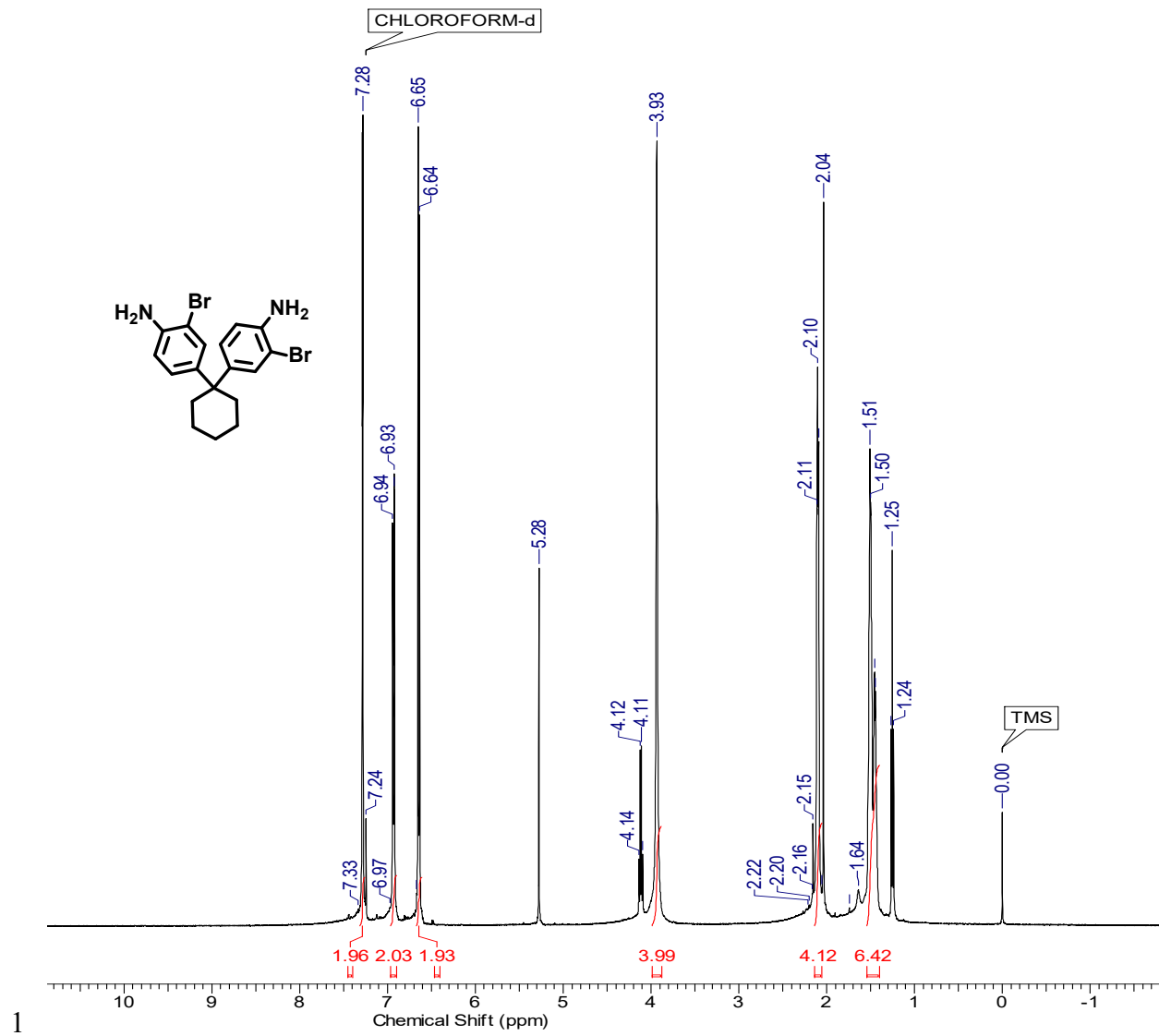
17 Density functional theory (DFT) and time-dependent density functional theory (TD-DFT)
18 calculations were performed using the Gaussian 16 software package with the B3LYP functional
19 and 6-31G(d) basis set. The polarizable continuum model with integral equation formalism
20 (IEPCM) was used for solvation (toluene). The HOMO and LUMO were obtained from the
21 optimized structures of the molecules in the ground state. The vertical excitation energies (S_1 and
22 T_n states) were obtained by calculating the Franck–Condon states from the ground state using TD-

1 DFT. In addition, the natural transition orbitals (NTOs) of the electronic transitions were calculated
2 to examine the electron and hole wavefunctions and characterize the electronic transition
3 properties.

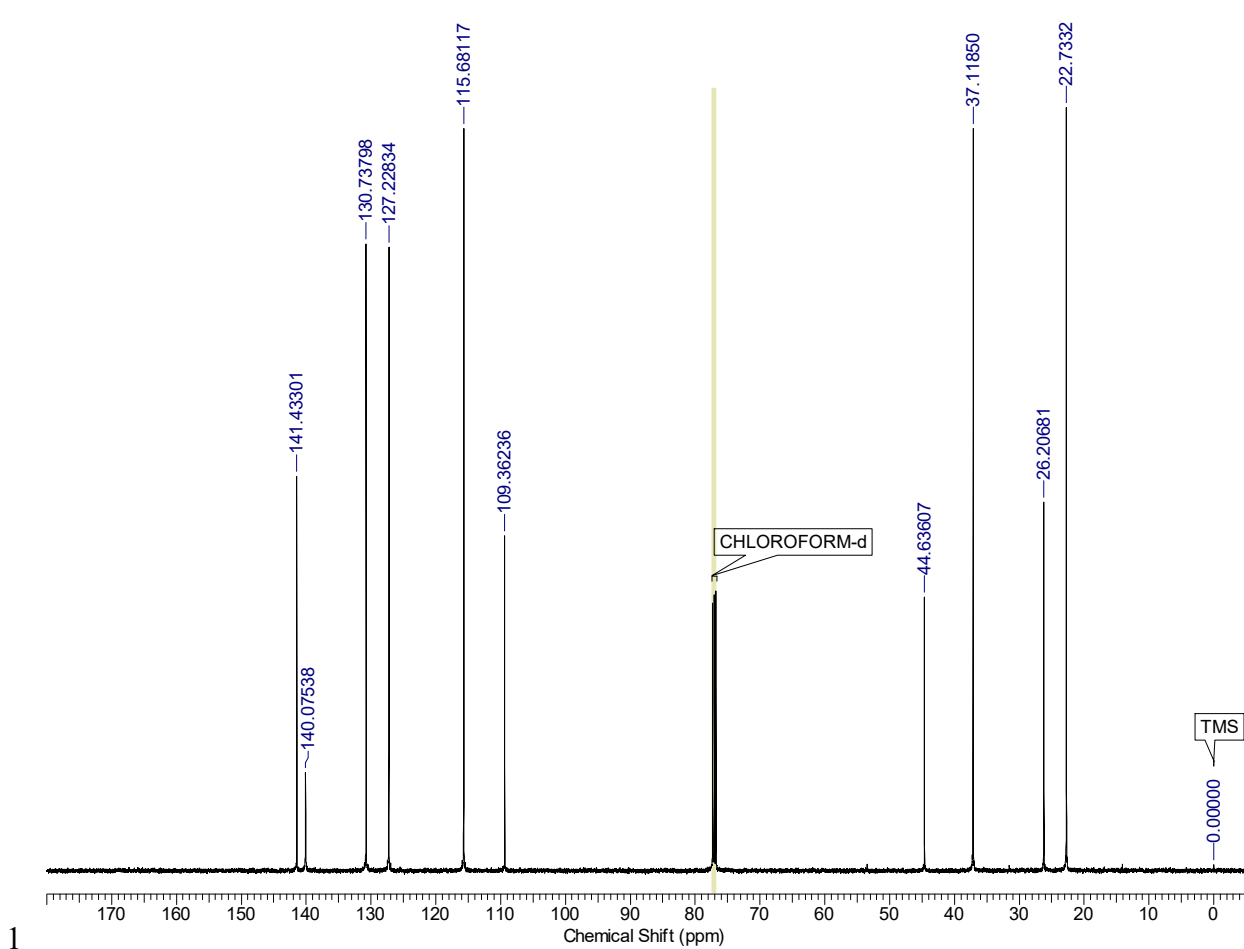
4

5 OLED device fabrication

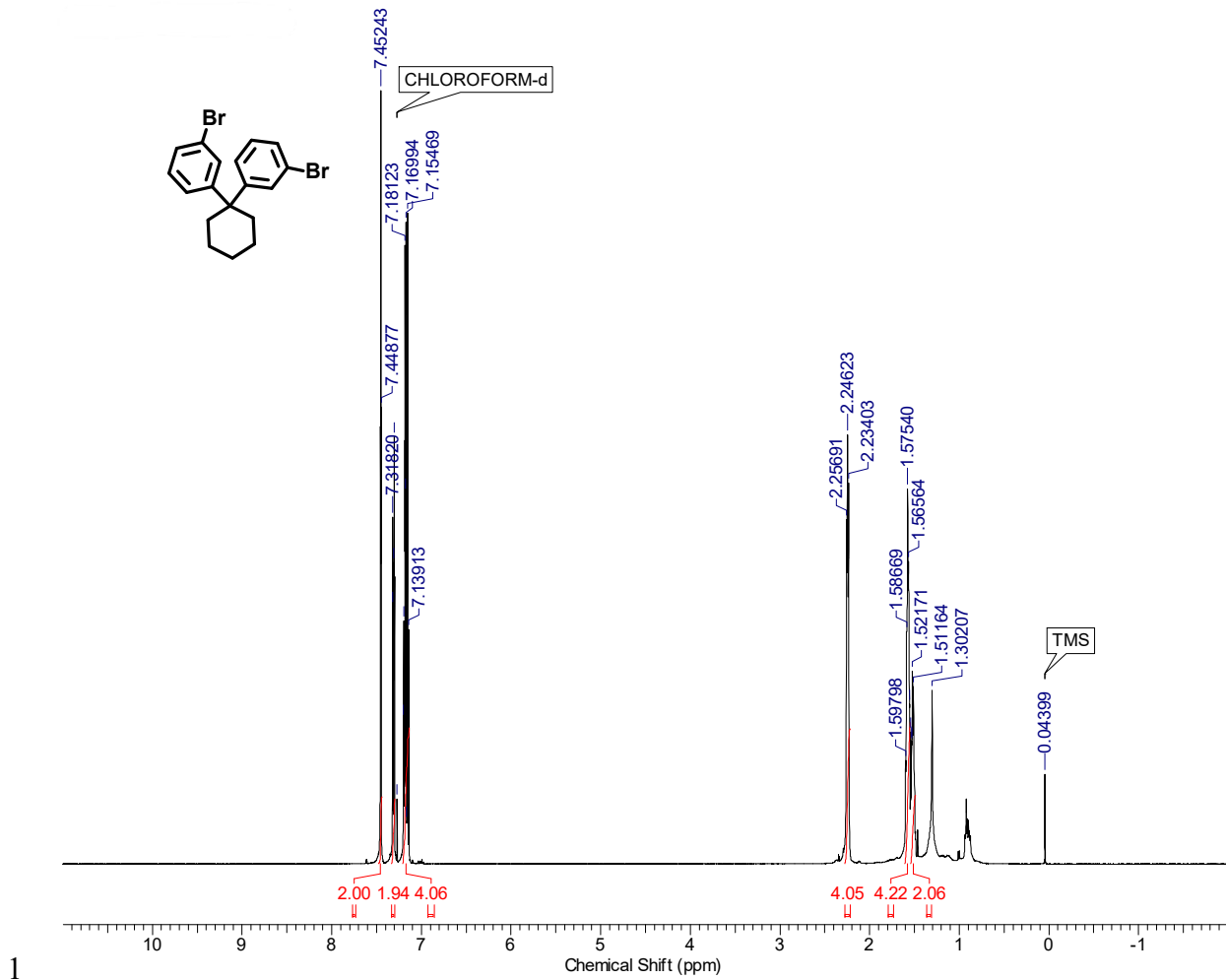
6 OLED devices were fabricated on a glass substrate coated with a transparent ITO layer (150 nm)
7 as the anode, with a sheet resistance of $15 \Omega \text{ cm}^{-2}$ and an active pattern size of $2 \times 2 \text{ mm}^2$. The
8 substrates were cleaned in distilled water for 10 min and isopropanol for 20 min using an ultrasonic
9 bath and subsequently dried using hot air. PEDOT:PSS was directly spin-coated onto an ITO plate
10 to form a hole injection layer (30 nm) and subsequently heated at 155°C for 15 min on a hot plate.
11 A mixture of hosts (CzCzPh-mAd, Cy-2(Ph-mCzCz), P(Ph-mCzCz)) and the 4FLDABNA emitter
12 (96:4 weight ratio, 0.5 wt.% in toluene) was spin-coated to fabricate the emitting layer. The
13 emissive layers (EMLs) were formed by spin-coating the solutions at 3000 rpm for 30 seconds.
14 The thickness of the EML layers was measured using a spectroscopic ellipsometer (Woollam
15 Alpha-SE), and found to be approximately 30 nm. BmPyPB (50 nm) was used as the electron-
16 transporting layer, and LiF (1 nm) and Al (100 nm) were vacuum-deposited in an inert chamber
17 under a pressure of 5×10^{-6} Torr. The fabricated device was constructed with the following
18 configuration: glass substrate/ITO anode/PEDOT:PSS (30 nm)/host: 4 wt.% 4FLDABNA (30
19 nm)/BmPyPB (50 nm)/LiF (1 nm)/Al (100 nm). Fabrication was performed under ambient
20 conditions before the substrates were placed in a thermal vacuum evaporator to evaporate
21 BmPyPB, LiF, and Al.



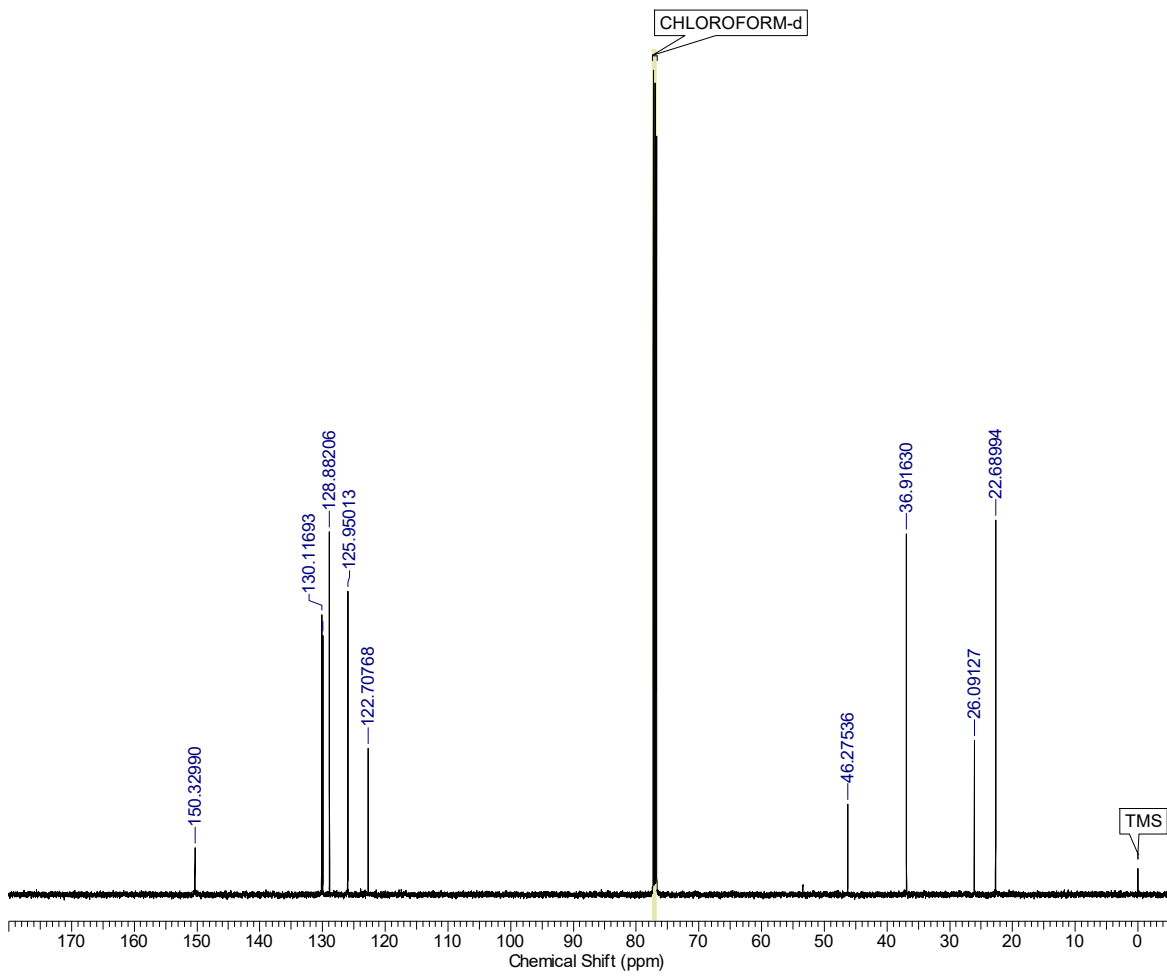
2 Fig. S1. ^1H NMR spectrum of 4,4'-(cyclohexane-1,1-diyl)bis(2-bromoaniline) (**2**)



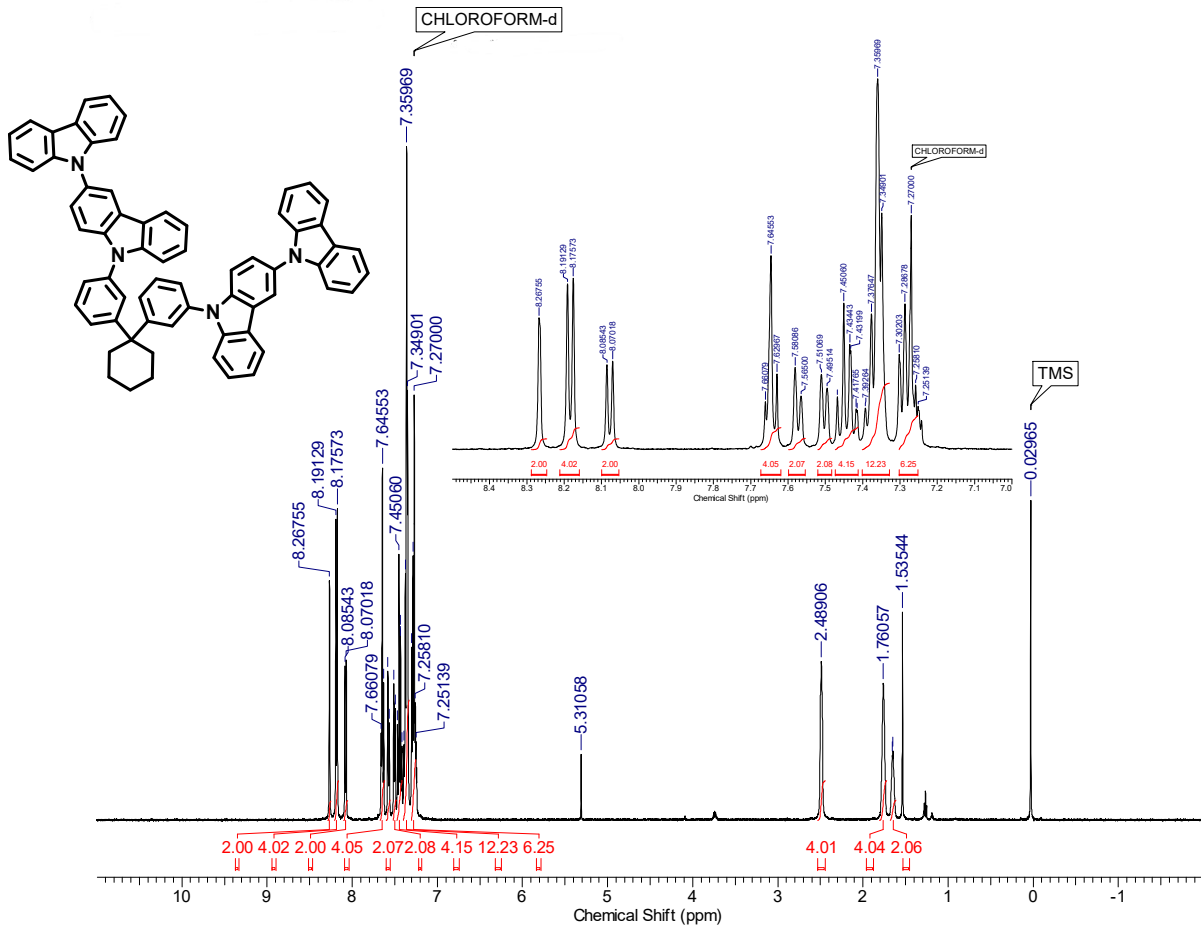
2 Fig. S2. ^{13}C NMR spectrum of 4,4'-(cyclohexane-1,1-diyl)bis(2-bromoaniline) (**2**)

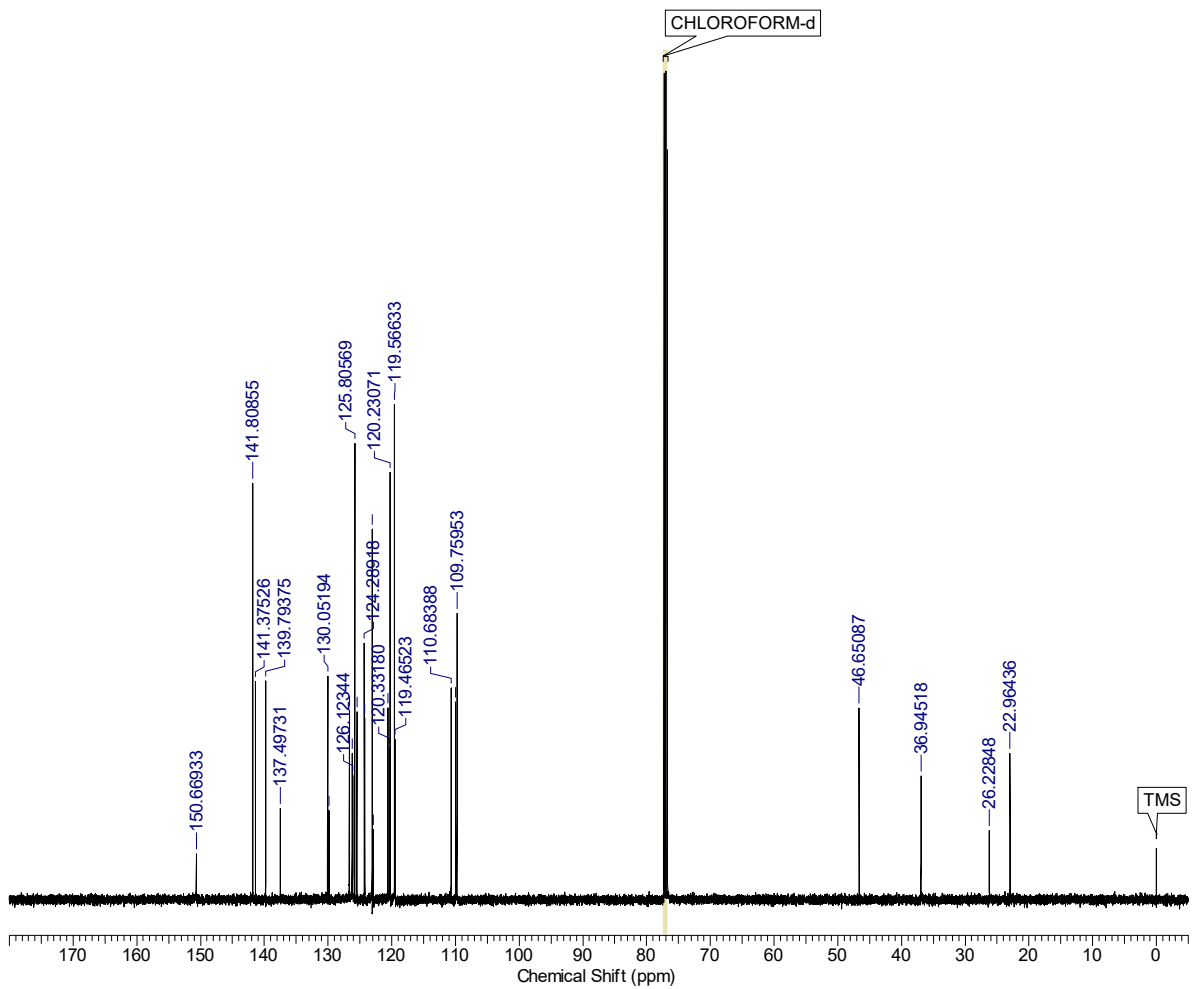


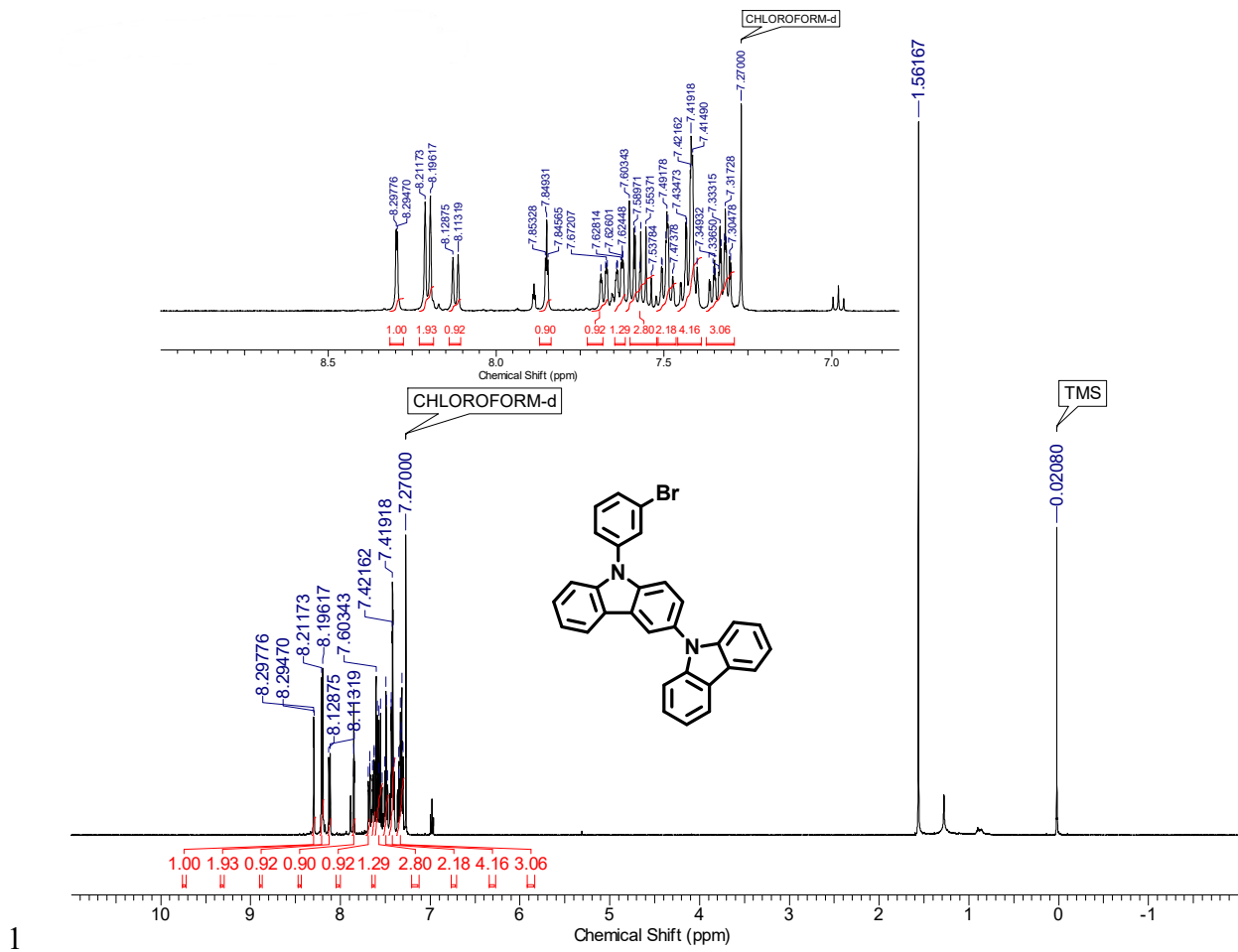
2 Fig. S3. ^1H NMR spectrum of 3,3-(cyclohexane-1,1-diyl)bis(bromobenzene) (**3**)



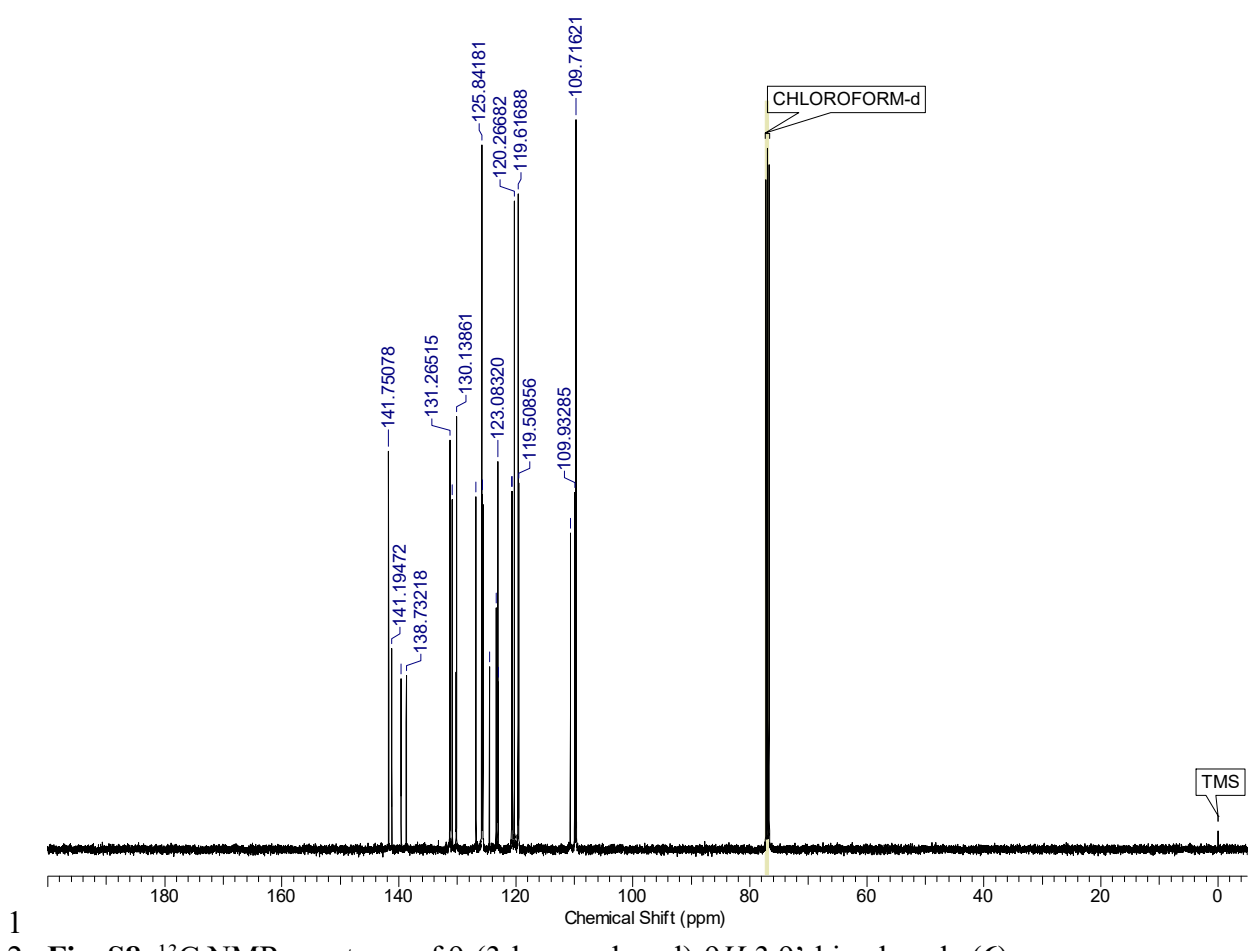
2 **Fig. S4.** ^{13}C NMR spectrum of 3,3-(cyclohexane-1,1-diyl)bis(bromobenzene) (**3**)







2 Fig. S7. ^1H NMR spectrum of 9-(3-bromophenyl)-9*H*-3,9'-bicarbazole (**6**)



1

2 **Fig. S8.** ^{13}C NMR spectrum of 9-(3-bromophenyl)-9*H*-3,9'-bicarbazole (**6**)

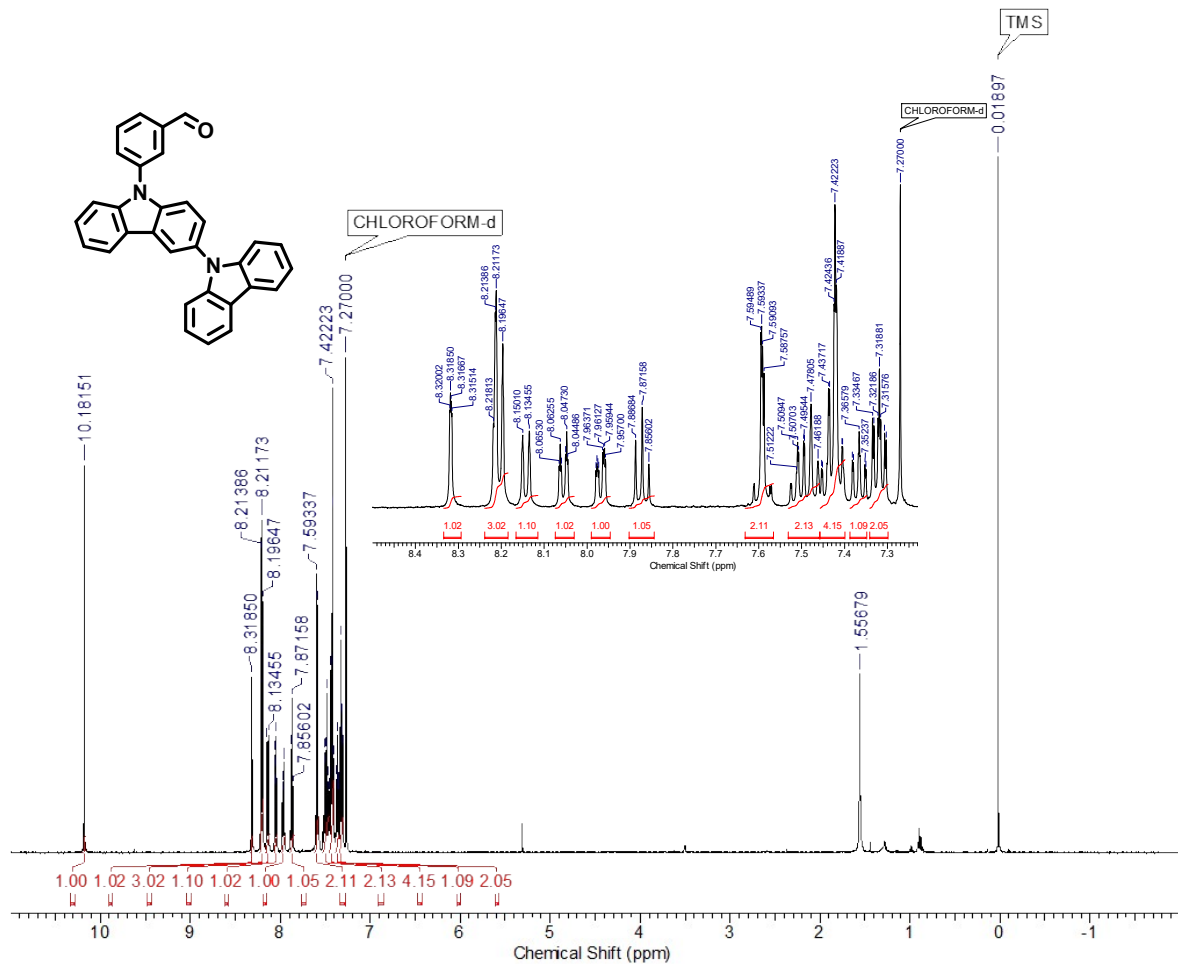
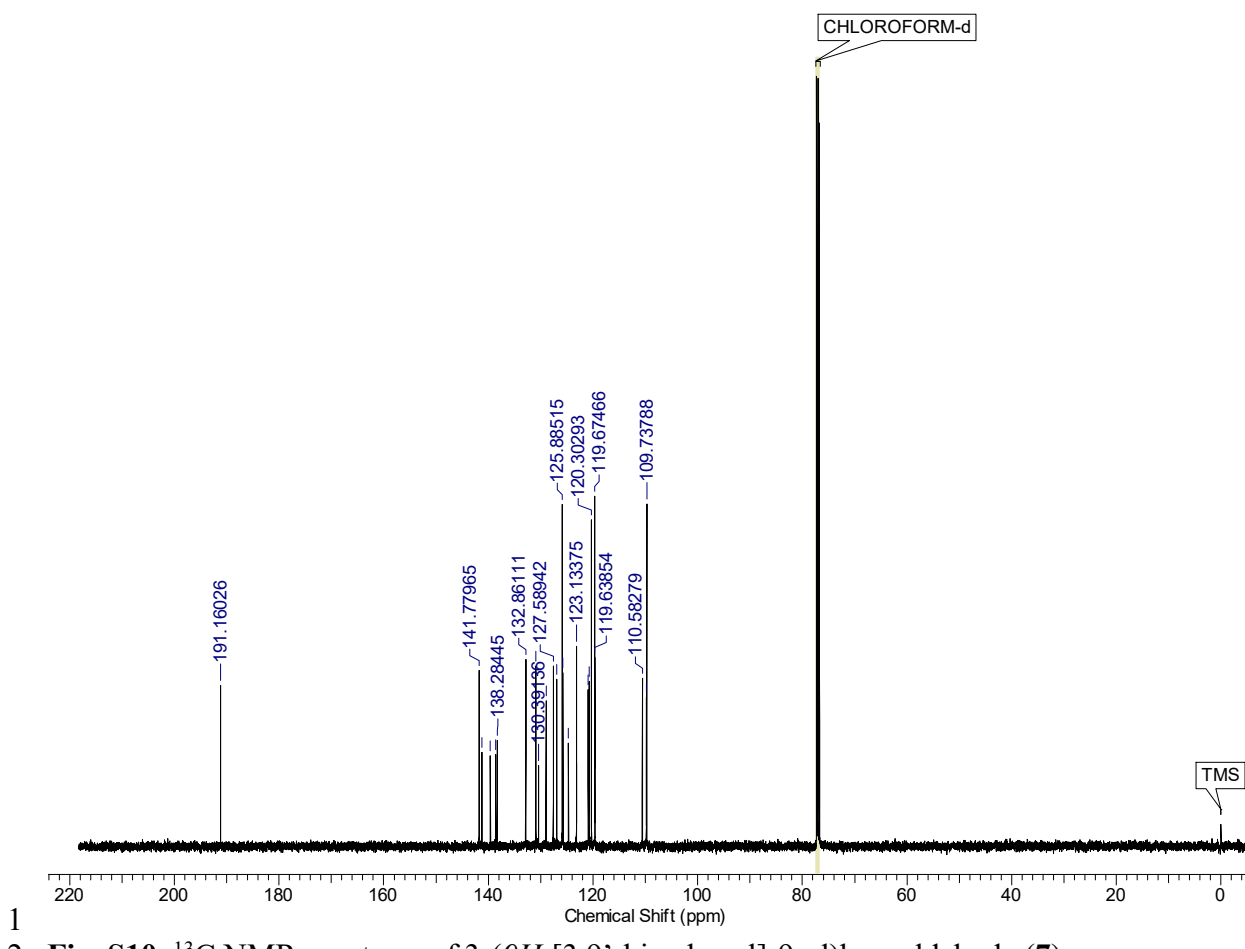


Fig. S9. ^1H NMR spectrum of 3-(9*H*-[3,9'-bicarbazol]-9-yl)benzaldehyde (7)



1

2 **Fig. S10.** ^{13}C NMR spectrum of 3-(9H-[3,9'-bicarbazol]-9-yl)benzaldehyde (**7**)

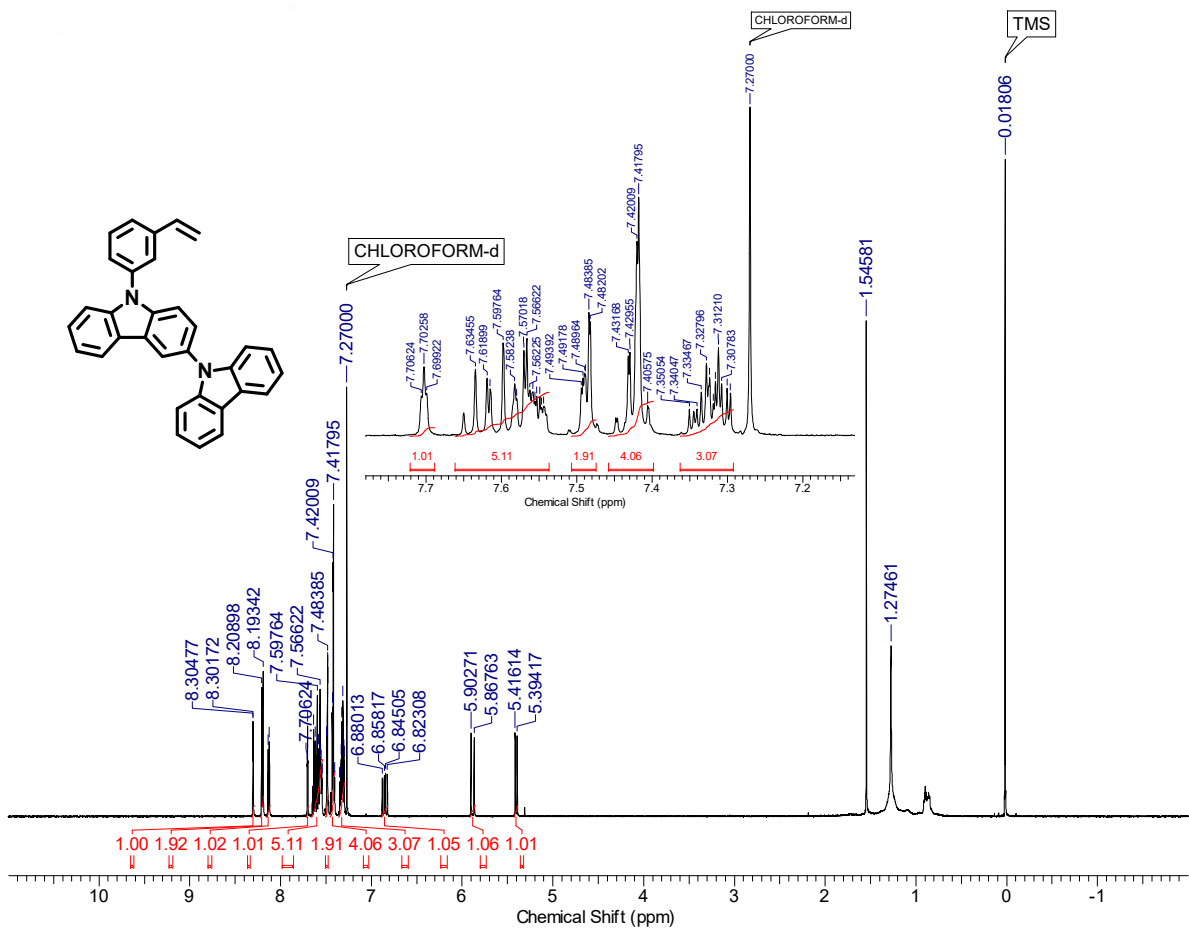
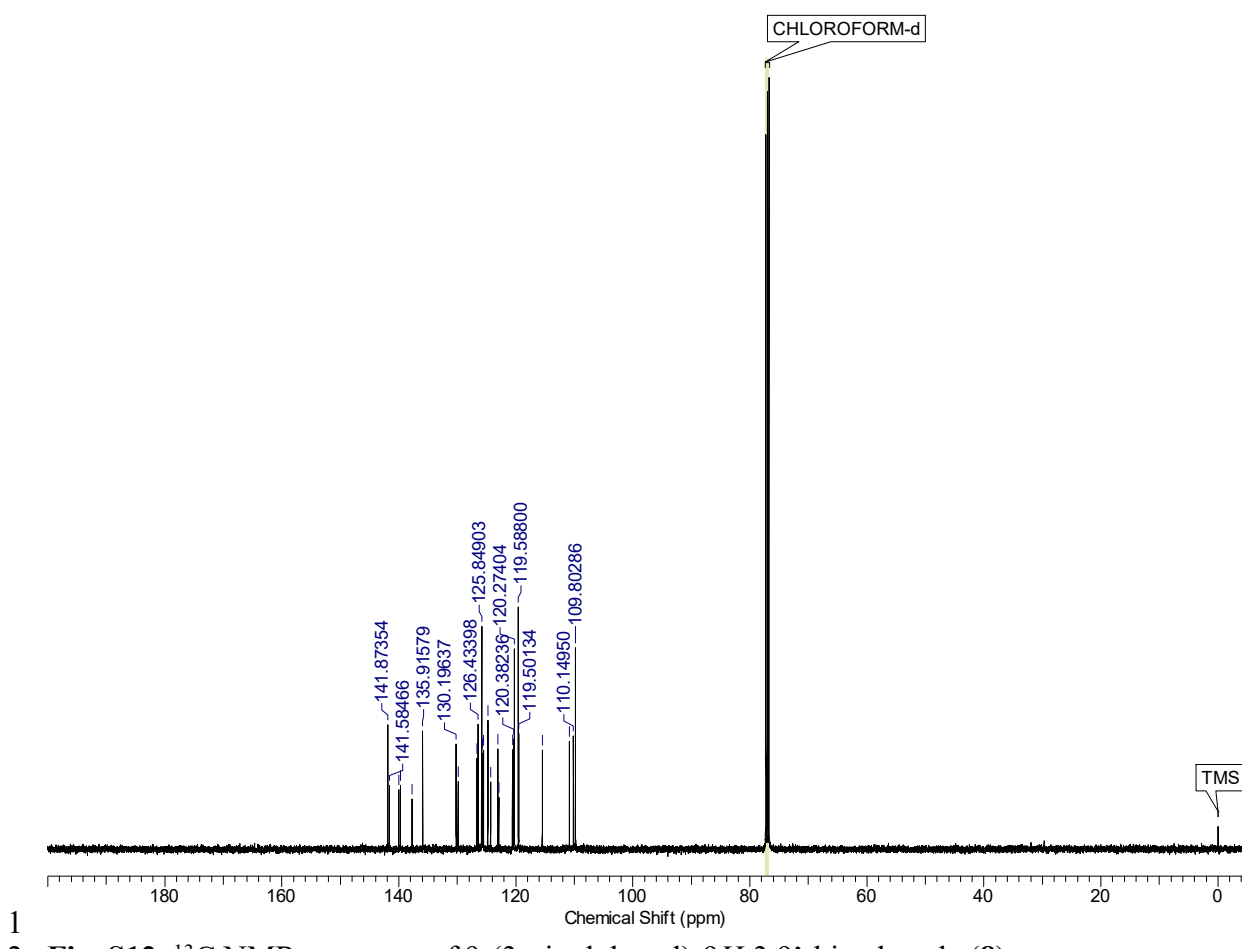
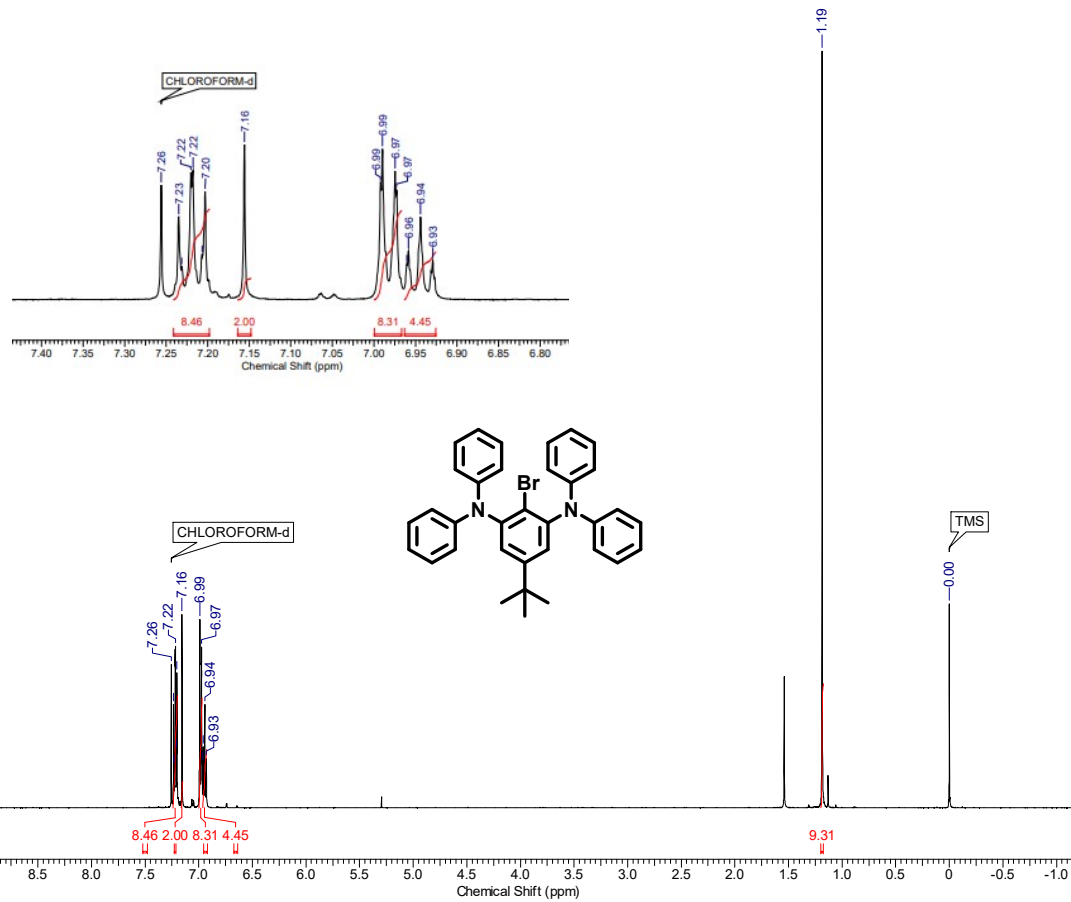
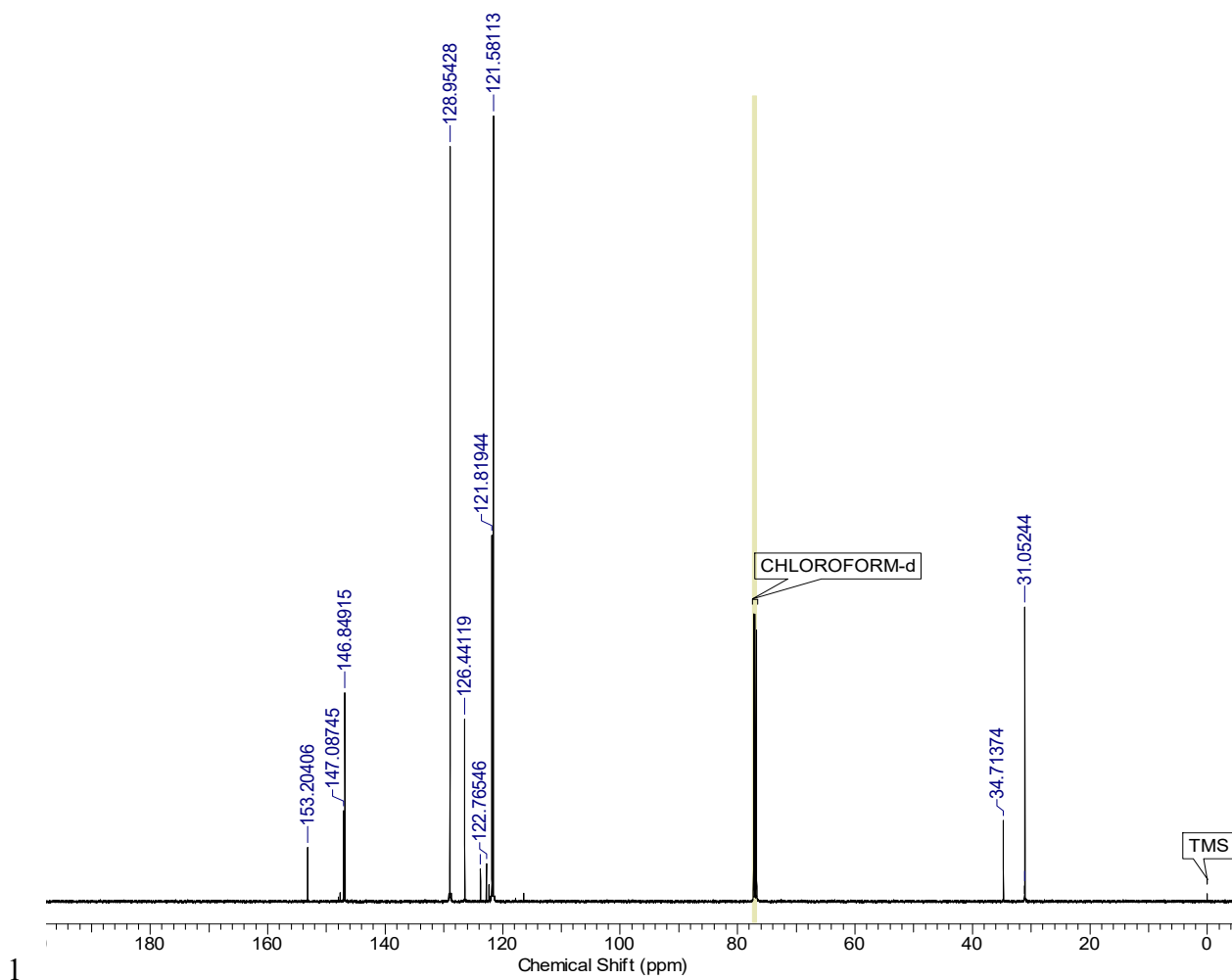


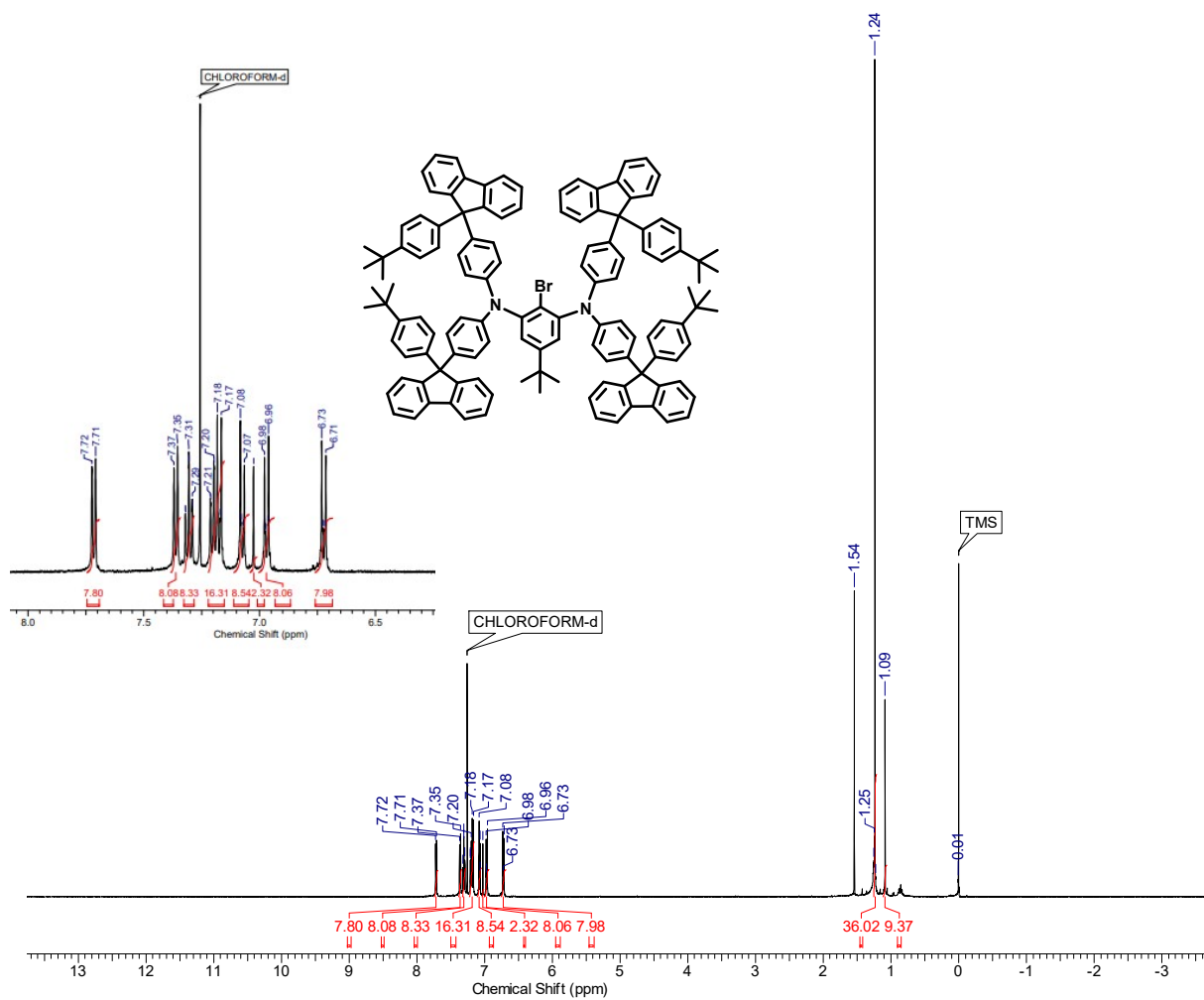
Fig. S11. ^1H NMR spectrum of 9-(3-vinylphenyl)-9*H*-3,9'-bicarbazole (**8**)



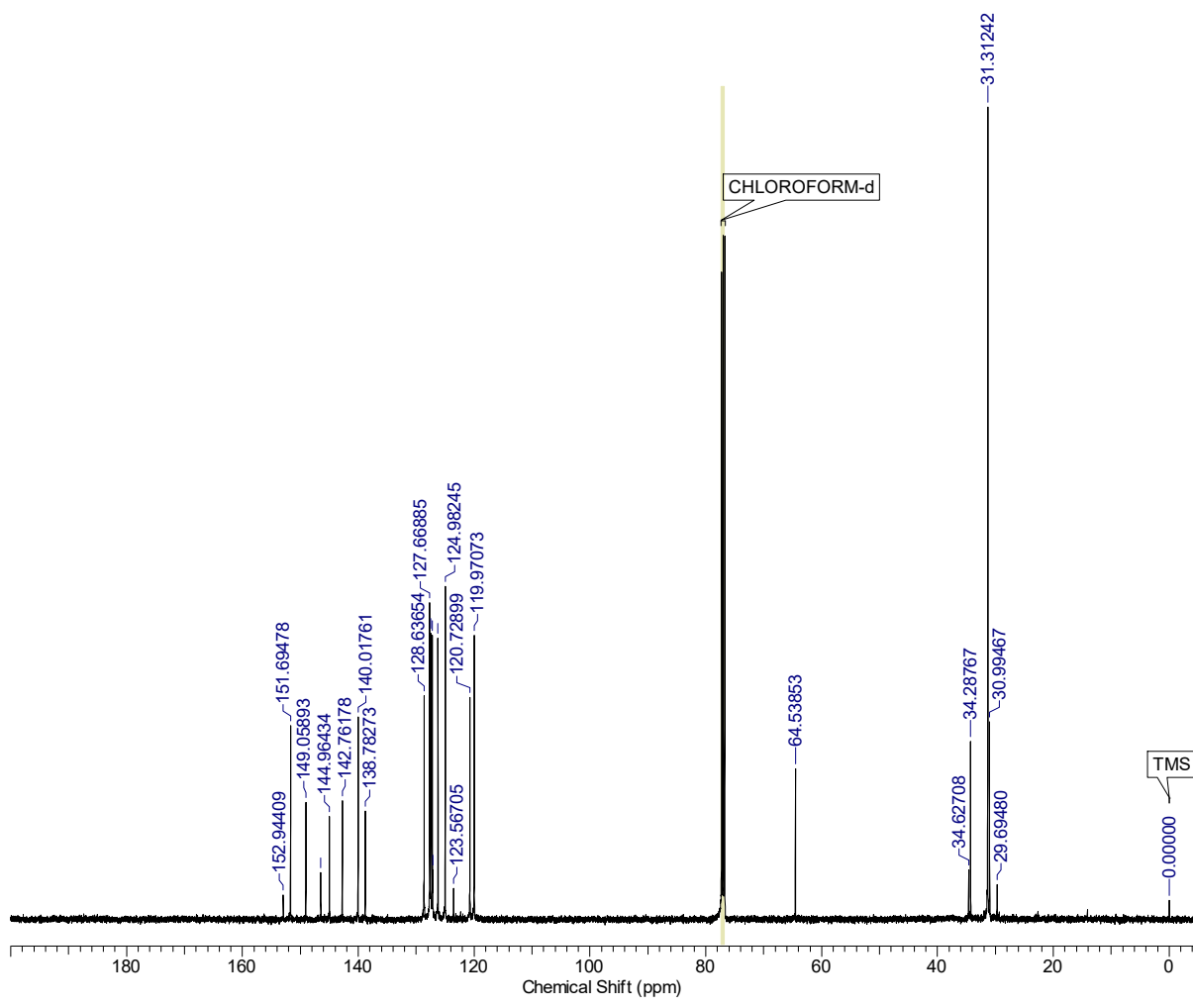


1
2 Fig. S13. ¹H NMR spectrum of 2-bromo-5-(*t*-butyl)-*N*¹,*N*¹,*N*³,*N*³-tetraphenylbenzene-1,3-
3 diamine (**11**)



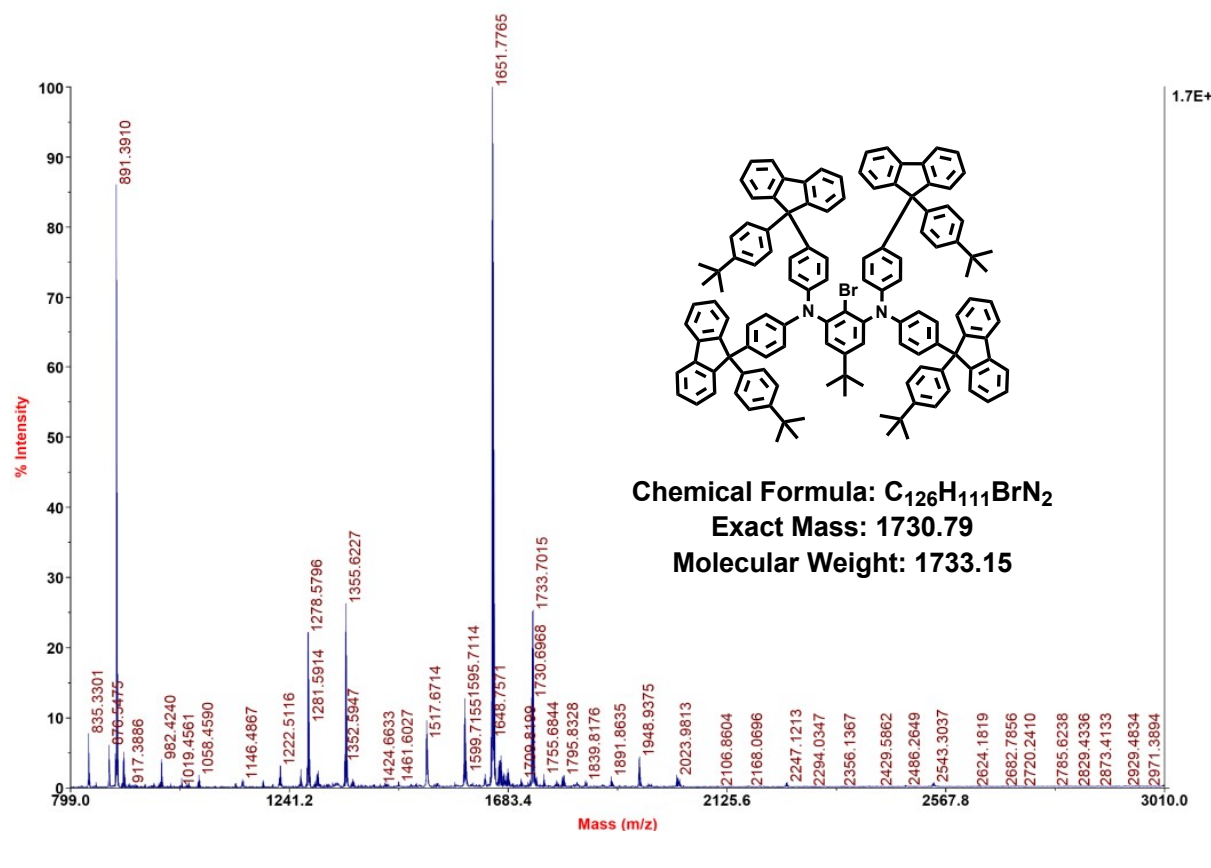


1
2 Fig. S15. ¹H NMR spectrum of 2-bromo-5-(*t*-butyl)-*N*¹,*N*¹,*N*³,*N*³-tetrakis(4-(9-(*t*-
3 butyl)phenyl)-9H-fluoren-9-yl)phenyl)benzene-1,3-diamine (**12**)
4



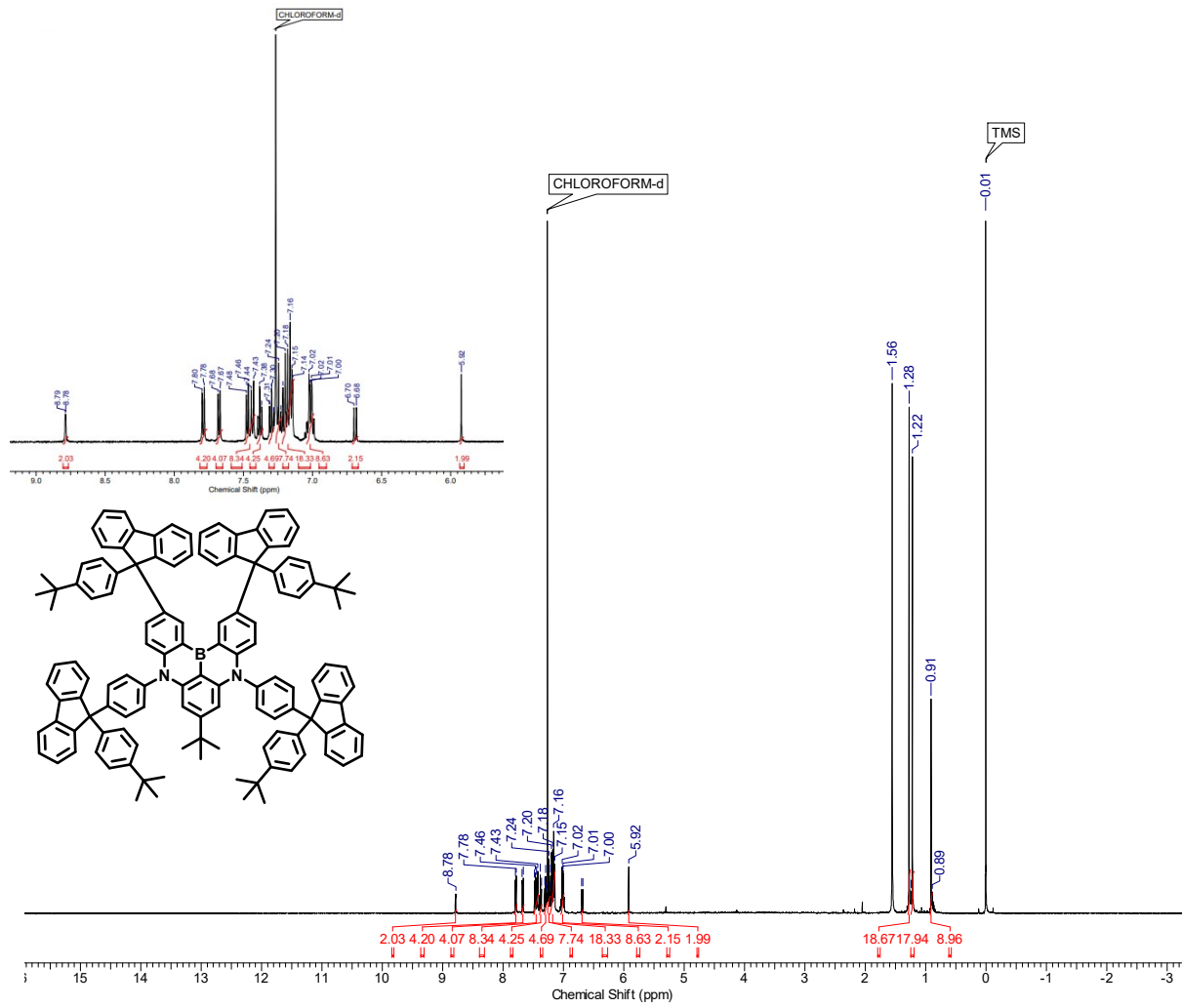
1
2 **Fig. S16.** ^{13}C NMR spectrum of 2-bromo-5-(*t*-butyl)- N^1,N^1,N^3,N^3 -tetrakis(4-(9-(*t*-
3 butyl)phenyl)-9H-fluoren-9-yl)phenyl)benzene-1,3-diamine (**12**)
4
5
6
7
8
9
10
11
12
13
14
15
16
17
18

TOF/TOF™ Reflector Spec #1 MC=>BC=>SM5[BP = 1651.8, 17190]

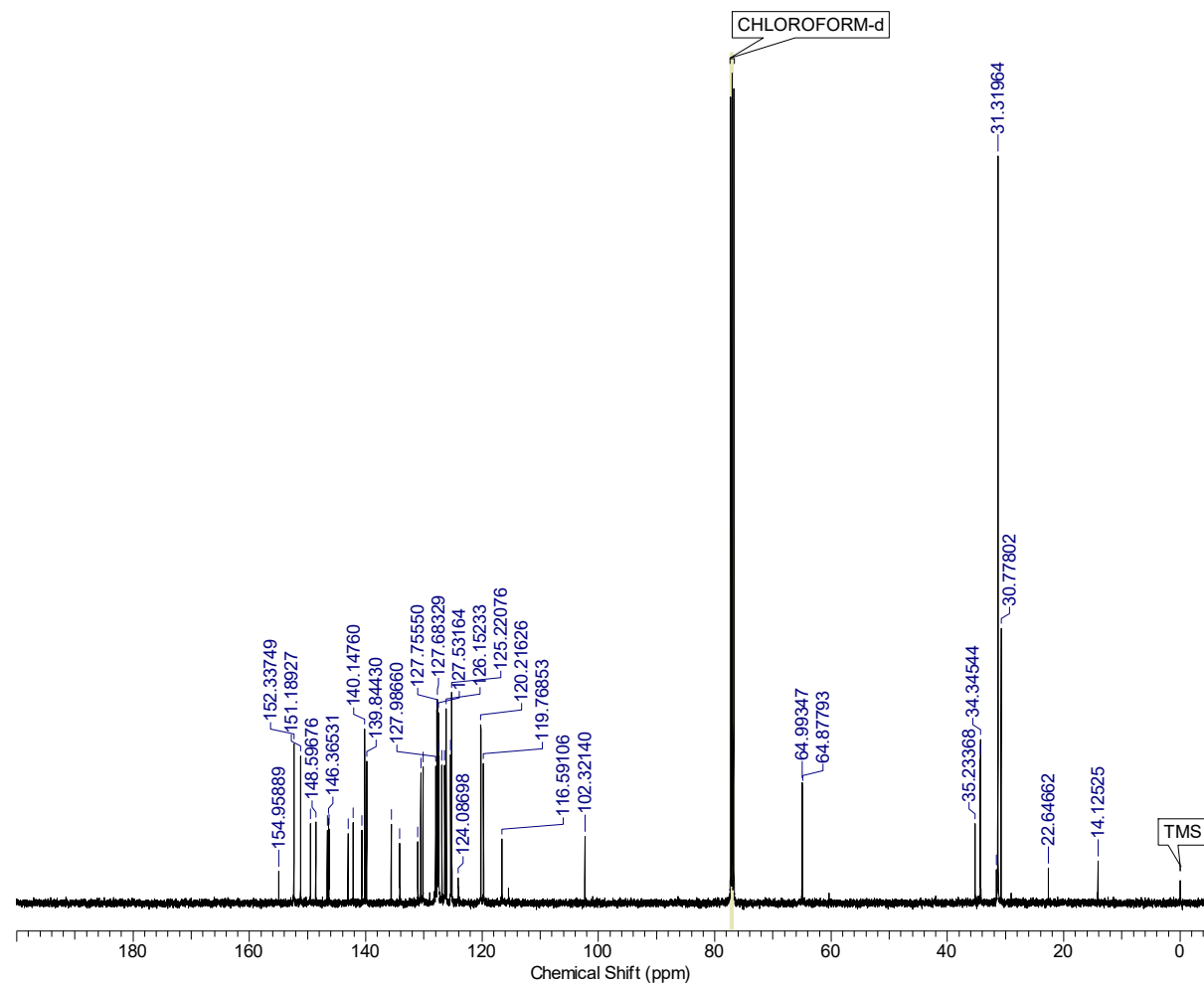


2 Fig. S17. MALDI-TOF mass spectrum of 2-bromo-5-(*t*-butyl)- N^1,N^1,N^3,N^3 -tetrakis(4-(9-(4-(*t*-butyl)phenyl)-9H-fluoren-9-yl)phenyl)benzene-1,3-diamine (**12**)

4
5
6
7
8
9

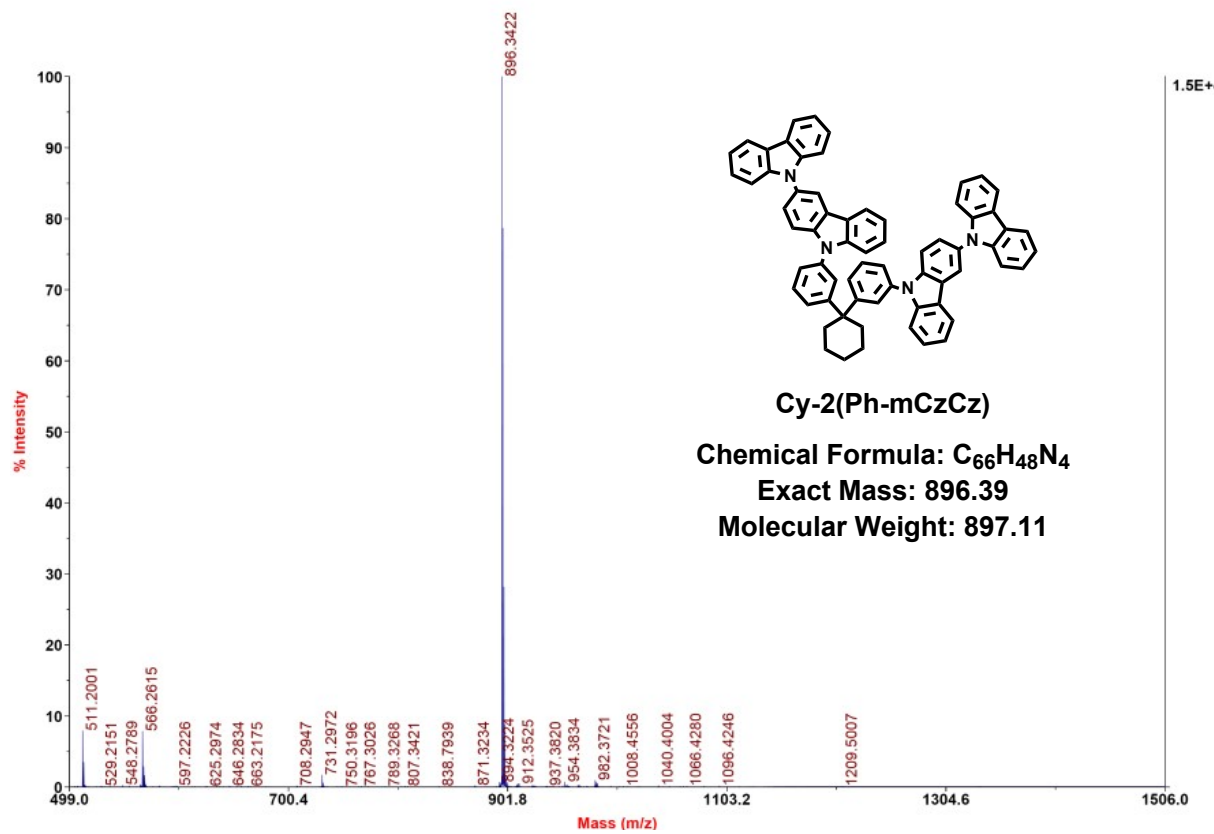


2 Fig. S18. ^1H NMR spectrum of 4FlDABNA (**13**)

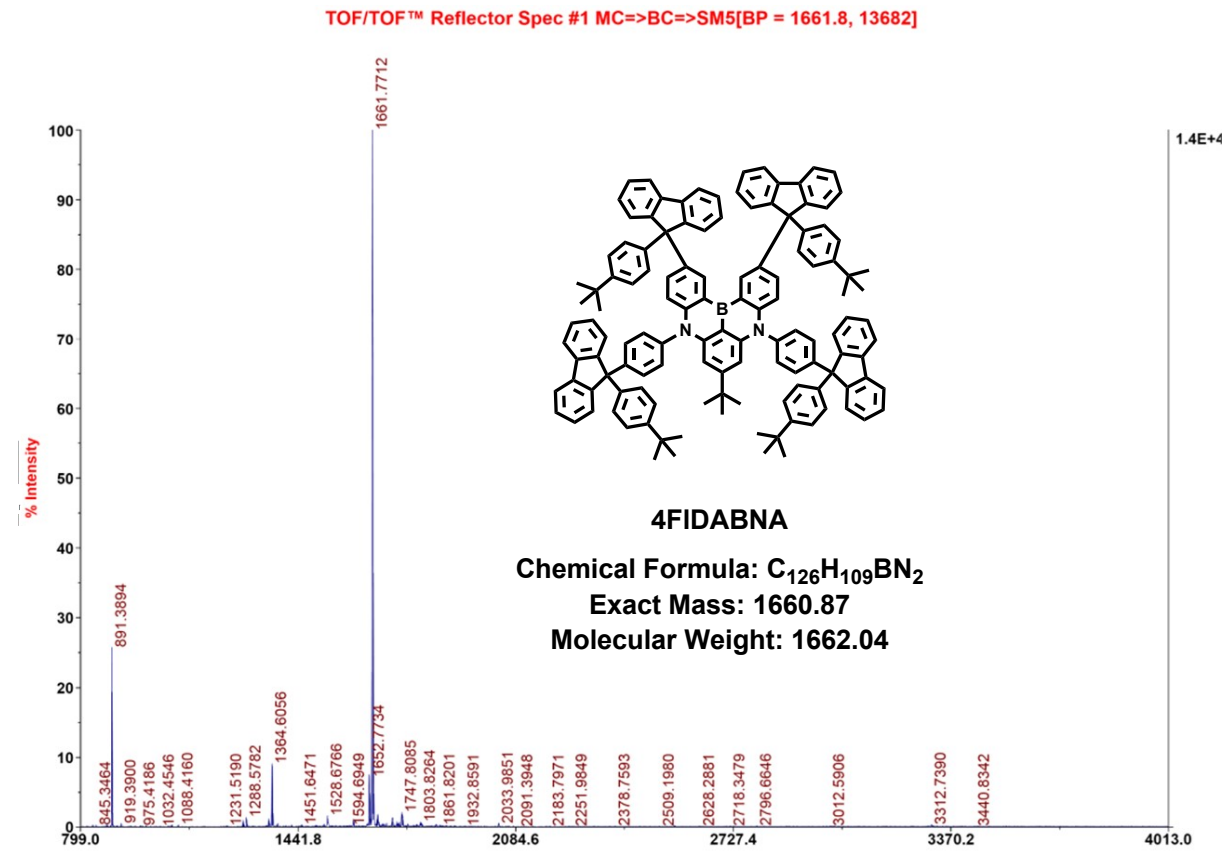


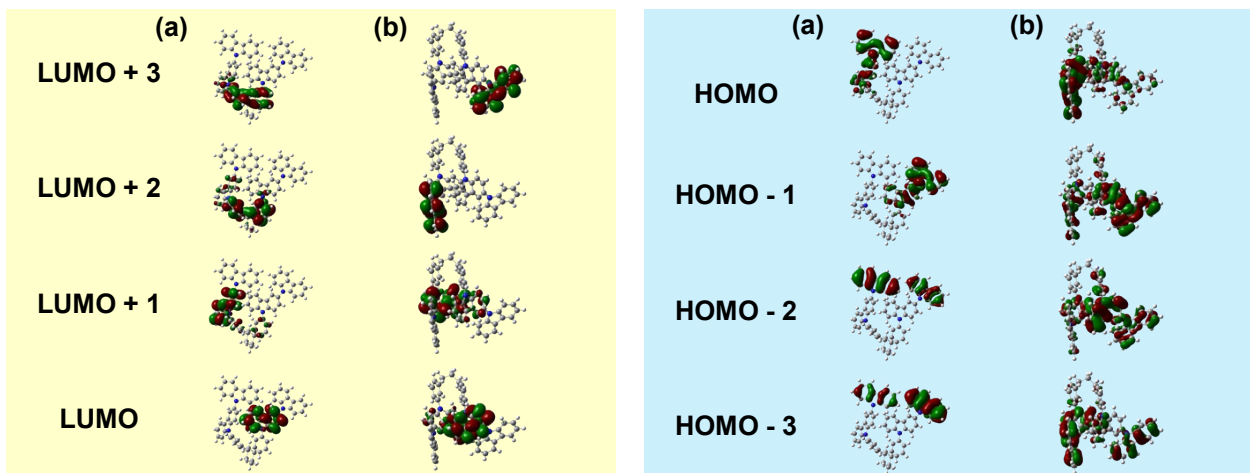
1
2 **Fig. S19.** ¹³C NMR spectrum of 4FlDABNA (**13**)

TOF/TOF™ Reflector Spec #1 MC=>BC=>SM5[BP = 896.3, 14580]



1
2 Fig. S20. MALDI-TOF mass spectrum of Cy-2(Ph-mCzCz) (4)
3





1
2 **Fig. S22.** Molecular orbitals of (a) Cy-2(Ph-mCzCz) and (b) P(Ph-mCzCz), as determined by
3 DFT calculations at the B3LYP/6-31G(d) level.

4

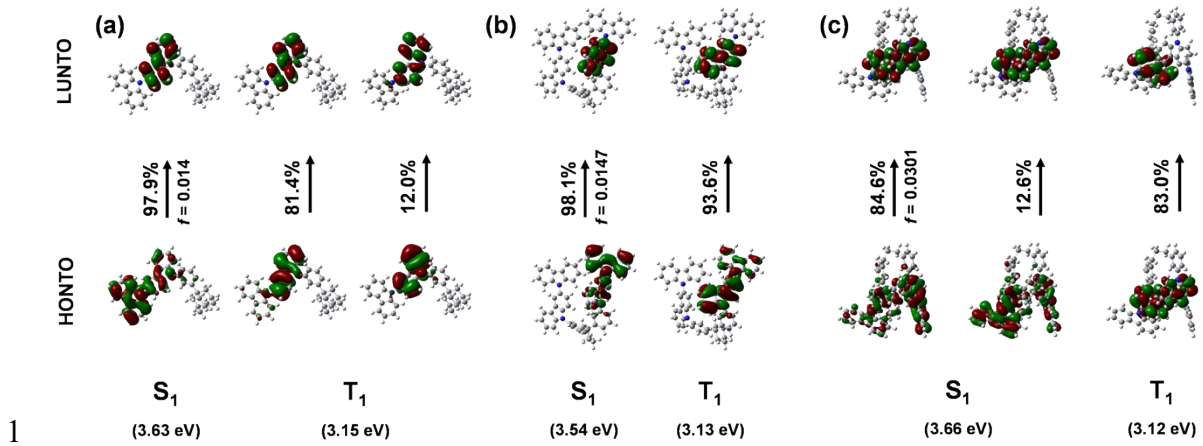
5

6 **Table S1.** Molecular orbital energies of Cy-2(Ph-mCzCz) and P(Ph-mCzCz), as determined by

7

Energy Level (eV)	Cy-2(Ph-mCzCz)	P(Ph-mCzCz)	DF T calc
LUMO+3	-0.70	0.72	ulati
LUMO+2	-0.82	-0.73	ons
LUMO+1	-0.87	-0.86	at
LUMO	-1.01	-0.86	the
HOMO	-5.01	-5.10	B3L
HOMO+1	-5.11	-5.15	YP/ 6-
HOMO+2	-5.54	-5.61	31G (d)
HOMO+3	-5.59	-5.75	leve
			l.

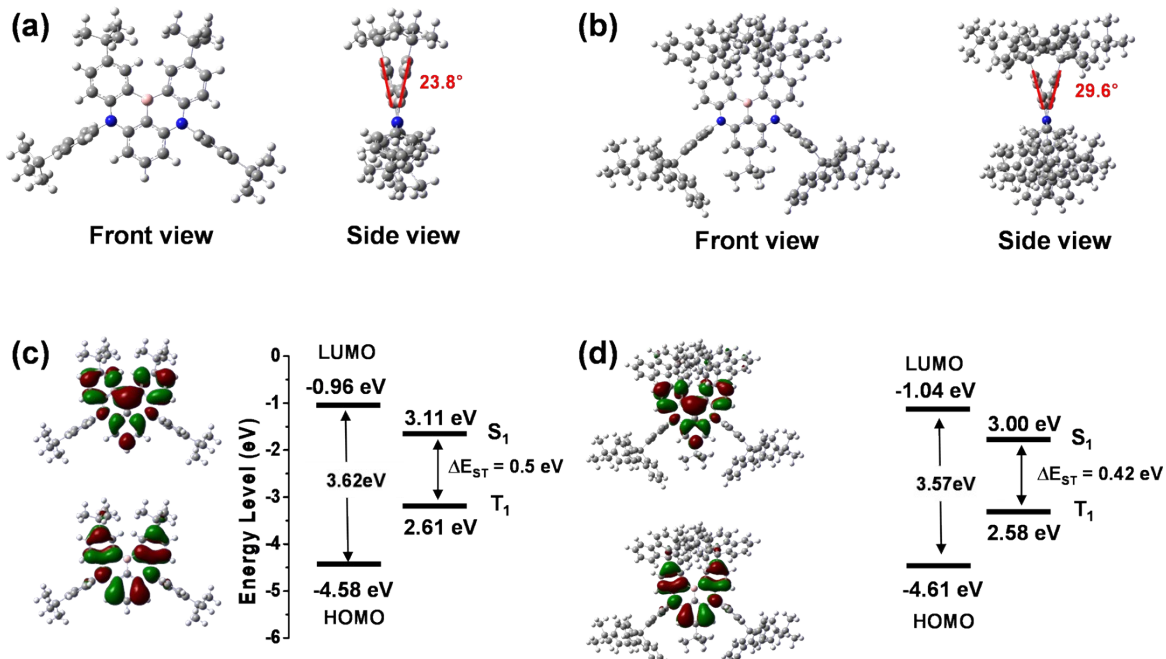
21



2 **Fig. S23.** Natural transition orbitals (NTOs) of (a) CzCzPh-mAd, (b) Cy-2(Ph-mCzCz) and (c)
3 P(Ph-mCzCz) for the excited singlet (S_1) and triplet (T_1) states obtained by DFT calculations
4 (B3LYP/6-31G(d)).

5

6



7

8 **Fig. S24.** Optimized molecular structures of (a) *t*-DABNA and (b) **4FIDABNA**, along with
9 HOMO and LUMO orbitals, S_1 , T_1 energy levels of (c) *t*-DABNA, and (d) **4FIDABNA**. The
10 energies were calculated using DFT at the B3LYP/6-31G(d,p) level.

11

12

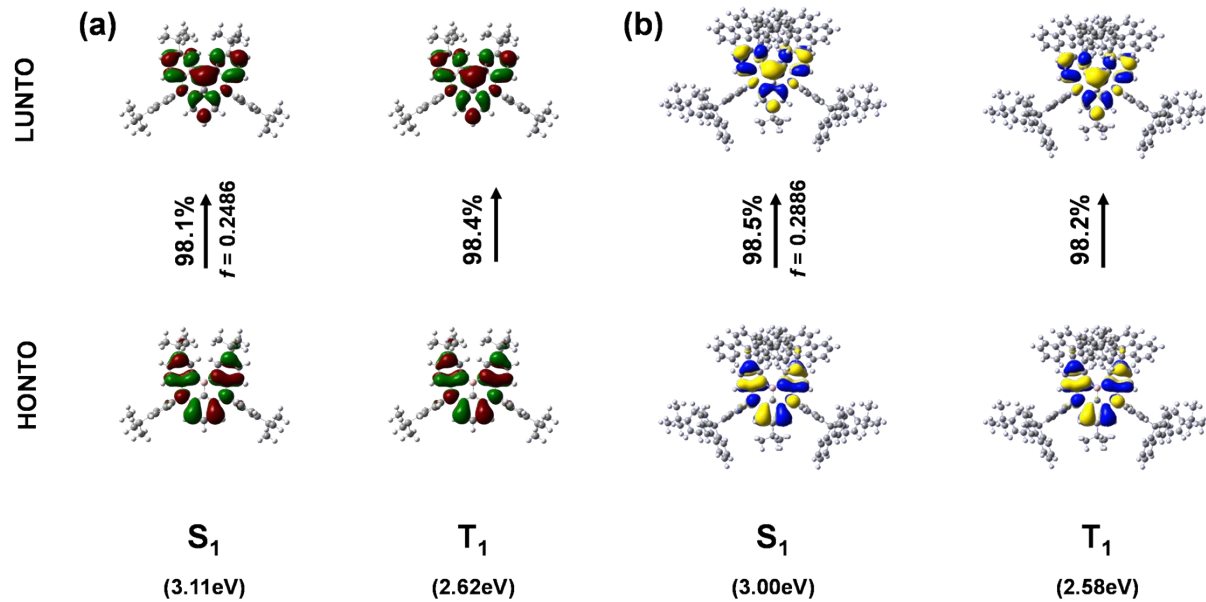
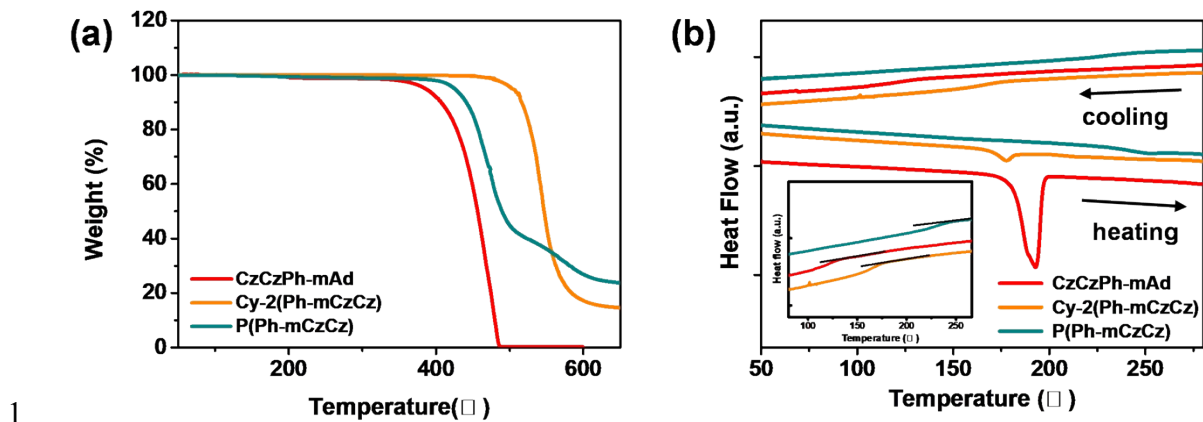


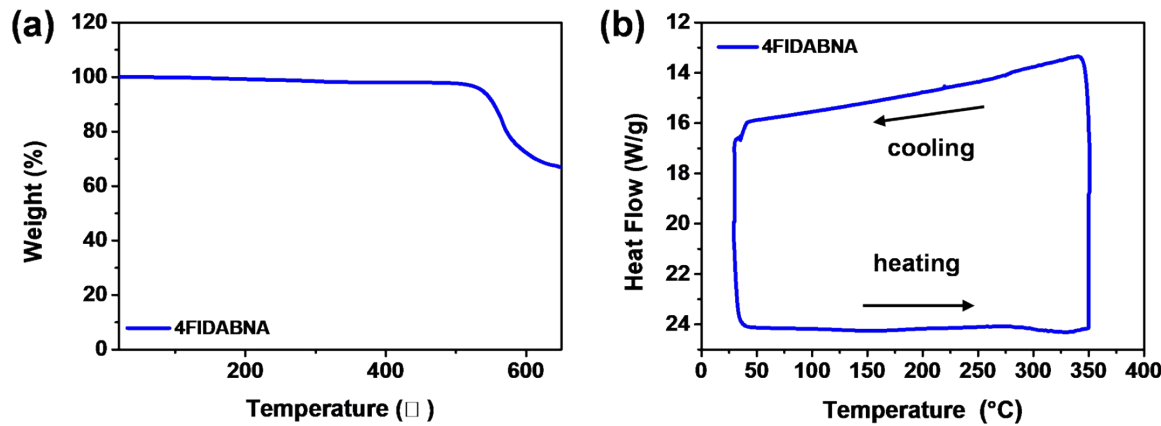
Fig. S25. Natural transition orbitals (NTOs) of (a) t-DABNA and (b) 4FIDABNA for the excited singlet (S_1) and triplet (T_1) states obtained by DFT calculations (B3LYP/6-31G(d)).



2 **Fig. S26.** (a) TGA thermograms and (b) DSC traces of CzCzPh-mAd, Cy-2(Ph-mCzCz), and
3 P(Ph-mCzCz) hosts, measured at a heating rate of 10 °C/min under a nitrogen atmosphere.

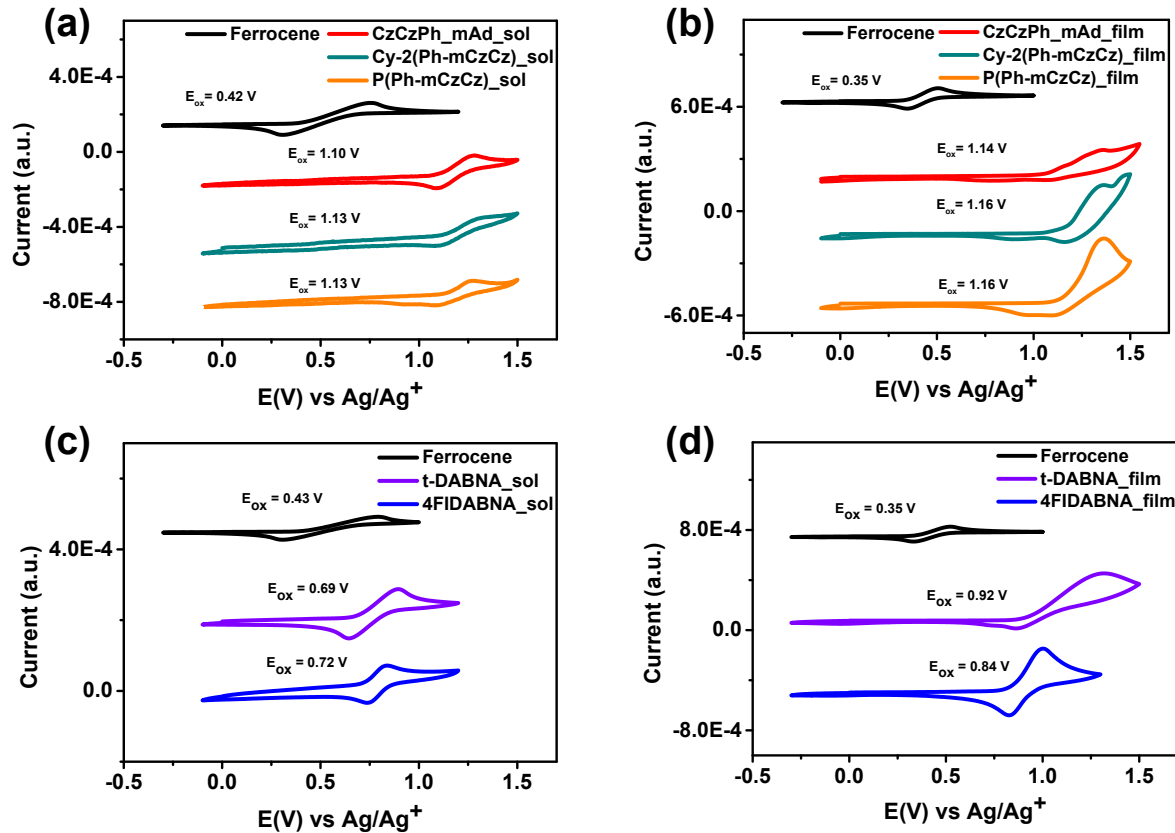
4

5



6

7 **Fig. S27.** (a) TGA thermograms and (b) DSC traces of 4FIDABNA, measured at a heating rate
8 of 10 °C/min under a nitrogen atmosphere.



1
2 **Fig. S28.** Cyclic voltammograms of the three host materials in (a) dichloromethane and (b) thin
3 films, and the two emitters in (c) dichloromethane and (d) thin films, respectively.
4

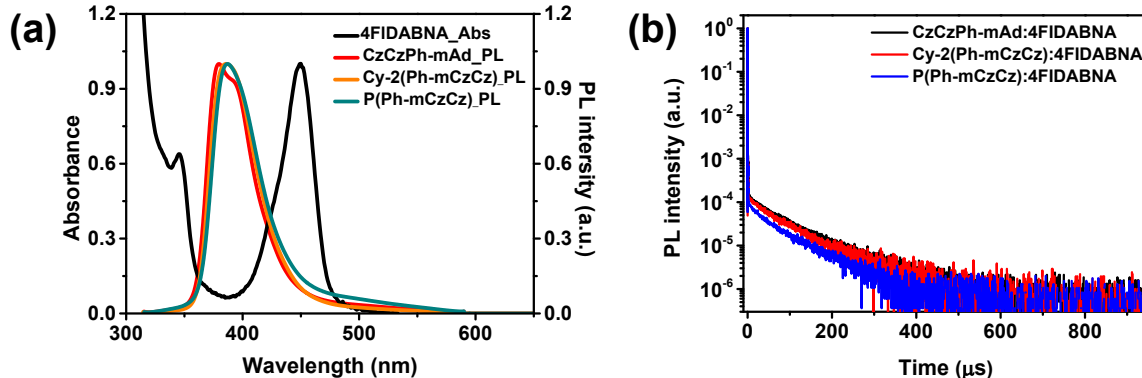
1 **Table S2.** Time-resolved photoluminescence (TRPL) properties and rate constants of neat and
2 films doped with 4FIDABNA.

	τ_1^a (ns)	τ_2^b (ns)	k_1^c ($\times 10^8 \text{ s}^{-1}$)	k_2^d ($\times 10^8 \text{ s}^{-1}$)	k_{FRET}^e ($\times 10^8 \text{ s}^{-1}$)	τ_{FRET}^f (ns)
CzCzPh-mAd	3.61	-	2.77	-	-	-
CzCzPh-mAd :4FIDABNA	-	1.87	-	5.35	2.58	3.88
Cy-2(Ph-mCzCz)	4.47	-	2.24	-	-	-
Cy-2(Ph-mCzCz) :4FIDABNA	-	2.12	-	4.72	2.48	4.03
P(Ph-mCzCz)	3.20	-	3.13	-	-	-
P(Ph-mCzCz) :4FIDABNA	-	2.00	-	4.99	1.86	5.38

3 ^a Host fluorescence lifetime of host. ^b Host fluorescence lifetime of host: 4 wt% 4FIDABNA. ^c Host fluorescence rate
4 constant of host. ^d Host fluorescence rate constant of host: 4 wt% 4FIDABNA. ^e Fluorescence Resonance Energy
5 Transfer rate constant. ^f Fluorescence Resonance Energy Transfer lifetime.

6

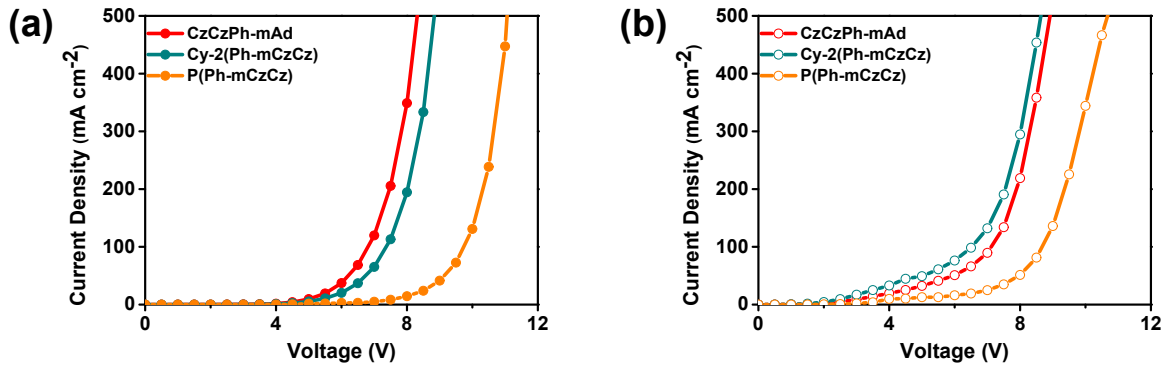
7



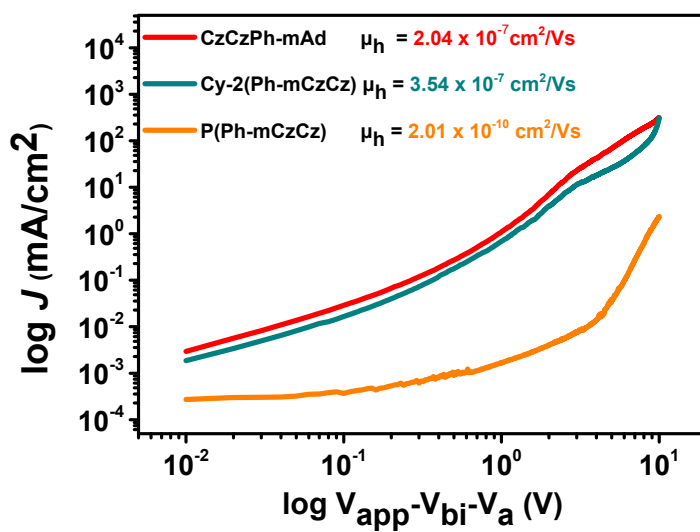
9 **Fig. S29.** (a) UV-vis absorption (Abs) and PL spectra of CzCzPh-mAd, Cy-
10 2(Ph-mCzCz), P(Ph-mCzCz) in film state. (b) TRPL signals were measured at 470 nm ($\lambda_{\text{ex}} =$
11 340 nm) for doped films.

12

13



1
2 **Fig. S30.** Current density–voltage (J – V) characteristics of (a) electron-only devices (EODs) and
3 (b) hole-only devices (HODs) for CzCzPh-mAd, Cy-2(Ph-mCzCz), and P(Ph-mCzCz) films
4 doped with 4 wt% 4FlDABNA.
5
6



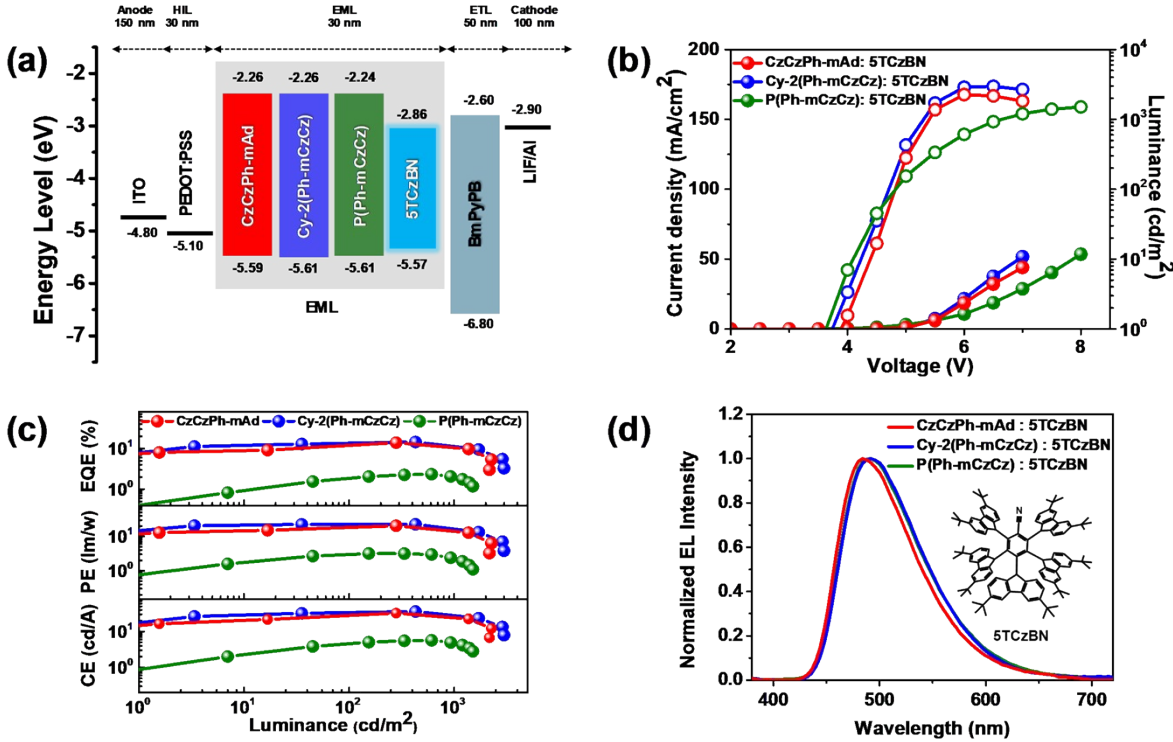
7
8 **Fig. S31.** Current density–voltage (J – V) characteristics of HODs based on CzCzPh-mAd, Cy-
9 2(Ph-mCzCz) and P(Ph-mCzCz). V_{app} : applied voltage to the device, V_{bi} : built-in potential
10 determined by the work-function difference between the two electrodes, V_a : voltage drop across
11 the device).

1 **Table S3.** Effect of drying time at 130°C on the electroluminescence performance of solution-
2 processed TADF-OLEDs using CzCzPh-based hosts doped with 4 wt% 4FlDABNA.

Drying Time at 130°C (min)	Host	Dopant	Doping Conc.	V_{on} (V)	CE max (cd/A)	PE max (lm/W)	Luminance (cd/m²)	EQE (%)	EL max (nm)	FWHM (nm)	CIE(xy) at 500 cd/m²
0	CzCzPhmAd	4FlDABNA	4 wt%	3.53	166	13.0	1692	148	472	287	(0.12, 0.14)
10	CzCzPhmAd	4FlDABNA	4 wt%	3.55	596	4.16	1562	556	468	292	(0.13, 0.14)
20	CzCzPhmAd	4FlDABNA	4 wt%	3.53	5.02	3.51	1480	459	472	290	(0.13, 0.14)
40	CzCzPhmAd	4FlDABNA	4 wt%	3.51	3.76	2.62	1408	352	472	288	(0.13, 0.15)
0	Cy-2(PhmCzCz)	4FlDABNA	4 wt%	3.51	17.7	13.9	1998	154	472	301	(0.12, 0.16)
10	Cy-2(PhmCzCz)	4FlDABNA	4 wt%	3.53	165	12.9	1451	13.7	472	302	(0.13, 0.15)
20	Cy-2(PhmCzCz)	4FlDABNA	4 wt%	3.51	13.3	10.5	1612	112	472	300	(0.13, 0.15)
40	Cy-2(PhmCzCz)	4FlDABNA	4 wt%	3.51	11.0	8.66	1572	935	472	303	(0.13, 0.15)
0	P(PhmCzCz)	4FlDABNA	4 wt%	4.17	3.52	2.76	4367	237	472	305	(0.14, 0.15)
10	P(PhmCzCz)	4FlDABNA	4 wt%	4.15	2.75	1.92	4938	232	472	32.6	(0.16, 0.15)
20	P(PhmCzCz)	4FlDABNA	4 wt%	4.14	2.60	1.82	469.1	231	472	322	(0.15, 0.15)
40	P(PhmCzCz)	4FlDABNA	4 wt%	4.05	3.01	2.10	4866	225	468	31.9	(0.15, 0.15)

3

4



1
2 **Fig. S32.** (a) Device configurations and energy diagram. (b) Current density–voltage–luminance
3 (J – V – L) characteristics. (c) EQE, power efficiency (PE), and current efficiency (CE) curves for
4 the devices. (d) Electroluminescence (EL) spectra of CzCzPh-based host films doped with 10
5 wt% 5TCzBN emitter. Inset: Emission image of the actual device.

6

7

8 **Table S4.** Electroluminescence (EL) performance of solution-processed TADF-OLEDs utilizing
9 CzCzPh-based hosts doped with 10 wt% 5TCzBN

Host	Dopant	V_{on} (V)	CE_{max} (cd/A)	PE_{max} (lm/W)	Luminance (cd/m ²)	EQE_{max} (%)	EL_{max} (nm)	CIE (x,y) at 1000 cd/m ²
CzCzPh-mAd		3.80	32.5	20.4	2265	13.9	484	(0.19, 0.37)
Cy-2(Ph-mCzCZ)	5TCzBN	3.61	35.9	22.6	2981	14.5	492	(0.21, 0.41)
P(Ph-mCzCZ)		3.54	3.16	2.34	1508	2.34	492	(0.20, 0.40)

10

11

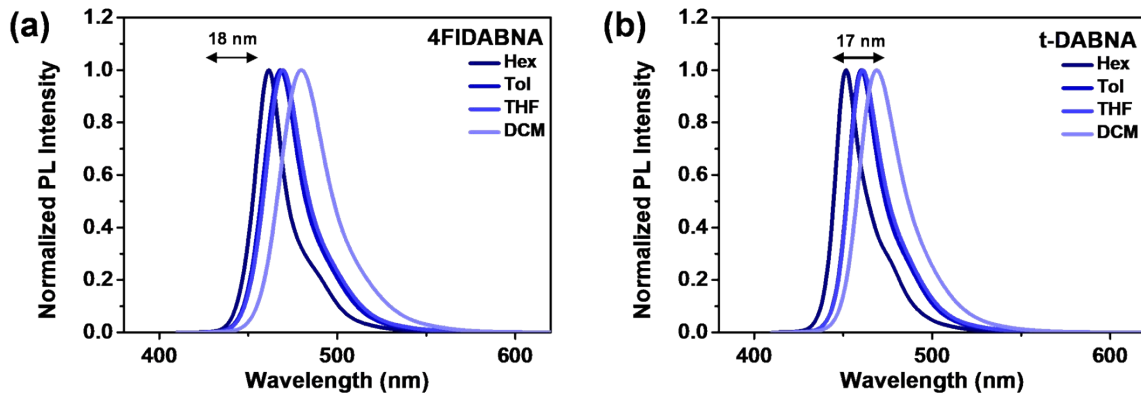
12

1 **Table S5.** Summary of EL performance of blue-emitting solution-processed OLEDs with a CIE
 2 y-coordinate below 0.2, as reported in the literature.

Device	Emitter Type	EQE _{max} (%)	λ_{EL} (nm)	FWHM (nm)	CIE(x,y)	REF
Cy-2(Ph-mCzCz): 4FIDABNA	MR-TADF	15.4	472	30	(0.12, 0.16)	This Work
PAc-BSS	MR-TADF	13.1	458	31	(0.16, 0.12)	S1
mCP: TBN-TPA	MR-TADF	1.08	464	32	(0.19, 0.19)	S2
mCP; TBN-TPA	MR-TADF	11.00	472	-	(0.12, 0.16)	S3
PYD2: Au-1:v-DABNA	MR-TADF	16.6	472	23	(0.14, 0.18)	S4
CzAcSF: CzBN	MR-TADF	14.7	480	35	-	S5
mCPCN: Me-FOBN	MR-TADF	11.3	458	32	(0.14, 0.09)	S6
H: S: D ₁	MR-TADF	9.68	467	18	(0.12, 0.13)	S7
CBP: 4CzFCN: KCTBC	TADF	13.9	-	-	(0.18, 0.13)	S8
mCP: TTSA	TADF	21.2	473	-	-	S9
mCP: TPA-s-Mes*B	TADF	10.3	454	-	(0.16, 0.12)	S10
PCzABTPy10	TADF	9.4	476	-	(0.17, 0.19)	S11
BOBTFB: TCTA	TADF	3.49	469	-	(0.15, 0.18)	S12

3

4



2 **Fig. S33.** Photoluminescence spectra of (a) 4FIDABNA and (b) *t*-DABNA in various solvents
3 (concentration: 1×10^{-5} M, 300 K).

4

5

6 **Table S6.** Summary of photoluminescence spectral data for 4FIDABNA and *t*-DABNA in various
7 solvents.

Solvent	4FIDABNA		<i>t</i> -DABNA	
	λ_{PL} (nm)	FWHM (nm)	λ_{PL} (nm)	FWHM (nm)
Hexane	462	20	452	20
Toluene	468	26	460	22
THF	469	26	461	23
DCM	480	32	469	29

8

9

1 References

- 2 S1. F. Chen, L. Zhao, X. Wang, Q. Yang, W. Li, H. Tian, S. Shao, L. Wang, X. Jing and F.
3 Wang, *Sci. China Chem.*, 2021, **64**, 547–551.
- 4 S2. S. K. Keshri, G. Liu and T. Yasuda, *Front. Chem.*, 2024, **12**, 1375552.
- 5 S3. H. Je, M. J. Cho, N. Y. Kwon, S. H. Park, M. J. Kang, H. I. Baek, J. Youn, C. W. Han and
6 D. H. Choi, *ACS Appl. Mater. Interfaces*, 2023, **15**, 9792–9799.
- 7 S4. D. Zhou, S. Wu, G. Cheng and C.-M. Che, *J. Mater. Chem. C*, 2022, **10**, 4590–4596.
- 8 S5. S. Xu, Q. Yang, Y. Zhang, H. Li, Q. Xue, G. Xie, M. Gu, J. Jin, L. Huang and R. Chen,
9 *Chin. Chem. Lett.*, 2021, **32**, 1372–1376.
- 10 S6. X. Song, S. Shen, Y. Zhang, S. Gao, F. Guo, Y. Wang, S. Zou, Y. Zhang, D. Zhang, Y.
11 Zhang *et al.*, *Adv. Opt. Mater.*, 2024, **12**, 2401505.
- 12 S7. H. W. Son, D. I. Kim, J. H. Kim, T. N. Le and M. C. Suh, *J. Ind. Eng. Chem. Res.*, 2025,
13 **141**, 512–520.
- 14 S8. M. I. Alam, M. R. Nagar, A. Choudhury, J.-H. Jou and S. Grigalevicius, *Adv. Opt. Mater.*,
15 2022, **10**, 2200376.
- 16 S9. M. Li, J. Jiang, Y. Ning and A. Al-Ghamdi, *Synth. Met.*, 2022, **289**, 117122.
- 17 S10. G. Liao, Y. Zhang, Z. Wang, B. Zhang, S. Zhang and Y. Li, *Adv. Opt. Mater.*, 2023, **11**,
18 2301242.
- 19 S11. H. Deng, B. Yao, K. K. Dou, Y. Y. Song, C. J. Qin, H. M. Zhan and Y. X. Cheng, *Acta
20 Polym. Sin.*, 2023, **54**, 217–224.
- 21 S12. J. Pan, S. Zhang, Z. Zhou, Y. Zhao, S. Jin, Y. Luo, W. Zhu and Y. Liu, *J. Mater. Chem. C*,
22 2025, **13**, 1165–1172.
- 23